THE EFFECT OF ZIRCONIUM ON THE LOW CYCLE FATIGUE BEHAVIOR OF AN ALUMINUM-ZINC-MAGNESIUM ALLOY

A THESIS

Presented to

The Faculty of the Division of Graduate Studies

by

Robert Edward Sanders, Jr.

In Partial Fulfillment

of the Requirements for the Degree

Master of Science in Metallurgy

Georgia Institute of Technology

June, 1976

THE EFFECT OF ZIRCONIUM ON THE LOW CYCLE FATIGUE BEHAVIOR

OF AN ALUMINUM-ZINC-MAGNESIUM ALLOY

Approved:

Dr. Edgar A. Starke, Jr., Chairman

Dr. Pieter Muije

Dr. Bruce G. Lefevre

Date Approved: 6/4/76

TABLE OF CONTENTS

		Page
ACKNOWLEDGEMENTS		ii
LIST OF FIGURES		iii
LIST OF TABLES		v
SUMMARY		vi
CHAPTER		
I.	INTRODUCTION	1
II.	REVIEW OF THE LITERATURE	3
	Effect of Grain Size on Fatigue Deviations in the Coffin-Manson Relation	
III.	EXPERIMENTAL PROCEDURES	12
IV.	EXPERIMENTAL RESULTS	16
V.	DISCUSSION OF RESULTS	42
VI.	CONCLUSIONS	57
APPENDIX		
A.	Low Cycle Fatigue Data for the Al-Zn-Mg-Zr Alloy	59
BIBLIOGRAPHY		60

ACKNOWLEDGEMENTS

The author would like to express his sincere appreciation to his thesis advisor, Dr. Edgar A. Starke, Jr. whose invaluable guidance made this work possible. He also wishes to thank Dr. B. G. LeFevre and Dr. P. Muije for their helpful suggestions in reviews of this work.

The helpful advice and suggestions of Dr. S. B. Chakrabortty, Dr. T. H. Sanders, Jr., and Dr. E. Y. Chen are deeply appreciated. Mr. Charles Blackwood of the Chemical Engineering and Metallurgy Machine Shop deserves much credit for the construction of apparatus and preparation of samples.

The author would also like to thank his colleagues and friends, particularly Ms. Rebecca Petty, for their assistance and support during this research. The capable typing of Mrs. G. Moore is gratefully acknowledged.

The author would like to thank the Alcoa Technical Center for preparing the alloys used in this investigation. The financial support of the Alcoa Foundation, the Air Force Office of Scientific Research, and the Graduate Division of the Georgia Institute of Technology is deeply appreciated.

LIST OF FIGURES

Figure		Page
1.	Microstructure of Al-Zn-Mg-Zr plate: (a) as-received, and (b) after solutionizing at 480°C for 1 1/2 hours. Anodized, 4% HBF_4.	17
2.	Subgrain Structure of the Al-Zn-Mg-Zr Plate: (a) and (b) as received, (c) and (d) after solutionizing at 480°C for 1 1/2 hours.	18
3.	Variation of Guinier Radius with Aging Time: (a) Al-Zn-Mg, and (b) 7050 (from the work of Sanders and Starke[4]).	21
4.	Low Cycle Fatigue Behavior of Al-Zn-Mg-Zr Aged 4 Hours at 120°C (4@120): (a) stress amplitude versus cycles, (b) Coffin-Manson plot, and (c) cyclic and monotonic stress-strain curves.	24
5.	Low Cycle Fatigue Behavior of Al-Zn-Mg-Zr Aged 24 Hours at 150°C (24@150): (a) stress amplitude versus cycles (b) Coffin-Manson Plot, and (c) cyclic and monotonic stress-strain curves.	25
6.	Low Cycle Fatigue Behavior of Double-Aged Al-Zn-Mg-Zr, 2 Hours at 120°C Followed by 12 Hours at 150°C (DA212): (a) stress amplitude versus cycles, (b) Coffin-Manson Plot, and (c) cyclic and monotonic stress-strain curves.	26
7.	Low Cycle Fatigue Behavior of Double-Aged Al-Zn-Mg-Zr, 12 Hours at 120°C Followed by 12 Hours at 150°C (DA1212): (a) stress amplitude versus cycles, (b) Coffin-Manson Plot, and (c) cyclic and monotonic stress-strain curves.	27
8.	Low Cycle Fatigue Behavior of Double-Aged Al-Zn-Mg-Zr, 24 Hours at 120°C Followed by 24 Hours at 150°C (DA2424): (a) stress amplitude versus cycles, (b) Coffin-Manson Plot, and (c) cyclic and monotonic stress-strain curves.	28
9.	Observations of Slip on Polished Surfaces of Tensile Samples: (a) Al-Zn-Mg , DA1212, (b) and (c) Al-Zn-Mg, 4@120, and (d) Al-Zn-Mg-Zr, 24@150.	31
10.	Observations of Slip Traces in Metallographic Sections of Al-Zn-Mg Tensile and Fatigue Specimens: (a) transverse section	

Figure Page

24@150 tensile, (b) transverse section 4@120 tensile, and (c) longitudinal section 24@150 fatigue, N_f = 141. 33

11. Observations of Tensile Fracture in the Two Alloys: (a) Al-Zn-Mg, DA1212, ε_f = 1.2%, 74X, and (b) overload area of Al-Zn-Mg-Zr, 24@150 fatigue specimen, $\Delta\varepsilon_p/2$ = 0.47% 112X. 34

12. Transmission Electron Micrographs of Transverse Sections of Fractured DA1212 Tensile Samples: (a) Al-Zn-Mg, ε_f = 1.2%, (b) and (c) Al-Zn-Mg-Zr, ε_f = 12.8%. 35

13. Macroscopic Scanning Fractographs of Typical 24@150 Fatigue Fracture Surfaces: (a) Al-Zn-Mg, $\Delta\varepsilon_p/2$ = 1.10%, 33X, and (b) Al-Zn-Mg-Zr, $\Delta\varepsilon_p/2$ = 0.47%, 30X. 37

14. Scanning Micrographs Showing Typical Fatigue Striations and Secondary Cracking in Al-Zn-Mg-Zr, 24@150 Fatigue Specimens: (a) $\Delta\varepsilon_p/2$ = 3.17%, 680X, and (b) $\Delta\varepsilon_p/2$ = 0.47%, 590X. 38

15. Polished and Anodized Longitudinal Section of Al-Zn-Mg-Zr Da2424 Tensile Sample Showing Fracture Surface and Associated Intergranular Cracks, 100X. 39

16. Cracking Associated with Slip Markings on the Surface of an Al-Zn-Mg-Zr 4@120 Fatigue Specimen, $\Delta\varepsilon_p/2$ = 4.27%. Scanning Electron Micrograph, 570X. 39

17. Typical Transmission Electron Micrographs of Al-Zn-Mg-Zr 24@150 Deformed Samples: (a) tensile, (b) fatigue, $\Delta\varepsilon_p/2$ = 6.38%, and (c) fatigue, $\Delta\varepsilon_p/2$ = 0.56%. 41

18. Effect of Grain Size Reduction by Zirconium Addition on LCF of Al-Zn-Mg-(Zr) for Two Aging Conditions: (a) 4@120, and (b) 24@150. 44

19. Effect of Aging Treatment on LCF Life of Al-Zn-Mg-Zr. 47

20. Comparison of LCF Data of Al-Zn-Mg-Zr and 7050 for Three Aging Conditions: (a) 4@120, (b) DA2424, and (c) 24@150. 51

21. Plot of Plastic Work versus Number of Cycles to Crack Initiation for: (a) 24@150, (b) 4@120 and (c) DA2424. 54

LIST OF TABLES

Table		Page
1.	Composition of the Aluminum Alloys	13
2.	Effect of Aging Treatment on Precipitate Size in Al-Zn-Mg-Zr, Al-Zn-Mg, and 7050	20
3.	Preliminary Tensile Data for Al-Zn-Mg-Zr and Al-Zn-Mg	23
4.	Tensile and Cyclic Properties of Al-Zn-Mg-Zr, Al-Zn-Mg, and 7050	30
5.	Comparison of Experimentally Obtained Fatigue Parameters with Various Theoretical Predictions	50

SUMMARY

The microstructure and low cycle fatigue behavior of an Al-Zn-Mg-Zr alloy were investigated and compared to the properties of a similar Al-Zn-Mg alloy determined previously.

The zirconium addition inhibited recrystallization during the solutionization heat treatment and resulted in an elongated, partially recrystallized microstructure. The grain size of the Al-Zn-Mg-Zr was reduced considerably compared to Al-Zn-Mg due to the presence of the zirconium as stable Al_3Zr in the microstructure. These precipitates were shown to have no effect on the aging kinetics in the Al-Zn-Mg-(Zr) system.

The large increase in ductility and elimination of brittle fracture in the Al-Zn-Mg-Zr alloy were attributed to the promotion of more homogeneous deformation by the refined grain structure. Brittle, intergranular fracture in aged Al-Zn-Mg tensile samples was caused by the presence of inhomogeneous deformation bands.

Improvements in LCF resistance were obtained in Al-Zn-Mg-Zr by an improved homogeneity of deformation which delayed crack initiation and failure. An overaged microstructure of large η particles obtained by aging for 24 hours at 150°C exhibited the best low cycle fatigue resistance observed in this study. The improved low cycle fatigue life of this aging treatment was attributed to the increased homogeneity of slip resulting from the occurrence of dislocation looping as the primary defor-

mation mechanism. Comparison of the Al-Zn-Mg-Zr low cycle fatigue data was made with existing data for a 7050 alloy, but complex microstructural differences between the two alloys prevented definitive conclusions. The break in the Coffin-Manson plot of low cycle fatigue data of samples aged for 24 hours at 150 °C was explained in terms of a change in the capacity of the microstructure to absorb energy prior to crack initiation at high and low plastic strain amplitudes.

CHAPTER I

INTRODUCTION

The development of precipitation hardened aluminum alloys has led to a considerable effort to obtain improvements in their fatigue properties[1]. Even though the high strength-to-weight ratio of these alloys has made them attractive to the aircraft industry, their susceptibility to fatigue has been a limiting factor in their applications thus far[2]. The widely used 7XXX (Al-Zn-Mg-Cu) series alloys have been shown to be especially poor in fatigue[3].

Because of the wide variety of precipitate structures obtainable in these alloys through age hardening, investigators have attempted to achieve improvements in fatigue properties through microstructure control. Results indicate that structures which reduce inhomogeneous deformation in these alloys are more resistant to fatigue[4]. A well-known means of promoting homogeneous deformation is a reduction in grain size. In Al-Zn-Mg-Cu alloys, the grain size is controlled by additions of ~0.1 per cent of chromium or zirconium. These elements form insoluble compounds with aluminum during casting and homogenization and act as grain refiners during subsequent heat treatment[1]. In studying the low cycle fatigue (LCF) response of these and other aluminum alloys, a number of investigators [3-10] have observed deviations from the well-known Coffin-Manson[5,6] relationship. Such behavior has been attributed to changes in deformation mode at low strain amplitudes[4,7], changes in crack propagation[8,9],

or strain localization effects [3,10]. The purpose of this study was to investigate the effects of a reduction in grain size and variation in aging treatment on the tensile and LCF behavior of two Al-Zn-Mg-(Zr) alloys.

CHAPTER II

REVIEW OF THE LITERATURE

Effect of Grain Size on Fatigue

Armstrong[11] has reviewed the early studies of the influence of grain size on the fatigue behavior of materials. Most of the results reported concern the effects of grain size on the familiar S-N curve. Sinclair and Craig[12] showed that the fatigue strength (σ_{FL}) of 70-30 brass was inversely proportional to mean grain diameter, d. Carreker[13] pointed out that their data could be interpreted easily using a σ_{FL}-$d^{-1/2}$ relationship similar to that for yielding[14]. Okubo et al.[15] confirmed these results while another investigation[16] showed that the fatigue limit of mild steel also obeys a Hall-Petch relation. However, the fatigue strengths of pure copper and aluminum have been found to be independent of grain size[17].

Feltner and Laird[18] have shown that the slip character of a material plays an important part in determining its fatigue response. Materials with a high stacking fault energy (SFE) are known to exhibit a wavy slip mode. Dislocations can cross slip easily and stable cell structures are formed during cyclic deformation[19,20]. Decreasing the SFE results in a planar slip mode with dislocations restricted to a single glide plane. Cross slip is extremely difficult and dislocations do not form cell structures, but planar bands[19,20]. Grosskreutz[21] further points out that lowering the SFE increases the reversibility of slip and

inihibits ease of crack initiation. In planar slip materials, slip is more reversible so that the development of the notch-peak topography known to precede crack initiation is delayed[22]. Partial or total slip irreversibility in high-SFE materials, due to the occurrence of cross slip, can hasten the appearance of intrusions and extrusions, leading to premature crack initiation and failure.

The concept of slip character is of great importance in explaining the grain size dependence of fatigue properties[23]. In materials where planar dislocation arrays are formed during cyclic deformation, grain boundaries act as obstacles, thus producing a microstructure dependent on the grain size. The size of the stable dislocation cells formed in wavy slip mode materials depends only on the applied strain amplitude[20] and is independent of grain size. Pelloux[23] has suggested that planar slip mode materials whose fatigue microstructure is affected by grain size should also show a grain-size dependence of its fatigue properties. A similar argument holds for wavy slip mode materials, supporting the observation of the grain size independence of pure copper and aluminum. The preceding argument, however, does not specify which particular fatigue event (i.e., crack initiation or crack propagation) is affected to produce the grain-size dependence of fatigue in planar slip materials.

More intensive research[24] has attributed the effect of grain size on high cycle, stress-controlled fatigue to the propagation of stage I cracks. Thompson and Backofen[24] showed that the average length of stage I cracks was related to the grain size in 70-30 brass but was independent of the grain size in pure copper. Through careful statistical

examination of crack populations and crack lengths, they were able to rule out the crack initiation process as the source of the grain size effect. They proposed that dislocations in the plastic zone of the stage I cracks in planar slip materials are not seriously impeded until a grain boundary is encountered. Stage I cracking proceeds further for larger grain sizes and fatigue life is shortened. For the wavy slip materials, e.g. copper, the dislocation cell structure of the persistent slip bands, in which stage I cracks begin, acts to eliminate the grain size effect. The cell walls, instead of grain boundaries, serve as slip barriers and hinder dislocation motion in the plastic zone of the growing stage I crack. Thus, for high cycle fatigue of wavy slip materials, the grain size is not a factor in determining the fatigue life.

There is significant evidence[25-75] that stage II propagation is not affected by grain size in either wavy or planar slip materials. Forrest and Tate[18] showed that, for pre-notched 70-30 brass specimens, in which stage II is immediate, there is no grain size effect. A recent investigation[1] has shown that a reduction in grain size may be detrimental to fatigue crack propagation (FCP) resistance in 2XXX and 7XXX series aluminum alloys. However, the changes in homogenization treatments used to vary the grain size in this study may also have affected other features of the microstructure known to influence FCP[3]. Regardless of the possiblilty of a grain size effect during stage II, this part of the fatigue process occupies only about 1 percent of total high cycle fatigue life ($>10^5$ cycles)[28,29].

The work of Feltner and Laird[19] has helped to clarify the role of grain size in high-strain low cycle fatigue (LCF). They found the

cyclic stress-strain response of pure copper to be unaffected by grain size. This result was not unexpected in view of the negligible effect of grain size on the unidirectional flow stress of copper[30]. They also suggested that a cyclic strain hardening exponent (n') of 0.15 should be applicable to all wavy slip materials, regardless of grain size. Another study[31] showed that the flow stress of copper cycled at constant strain amplitude was independent of grain size, a result attributed to the influence of the dislocation cell structure formed during fatigue. It was shown that the cyclic flow stress[31] and cyclic stress-strain curves[19] of planar slip Cu-7.5Al showed a marked grain-size dependence. The value of n' for Cu-7.5Al was found to be lower than that observed for pure copper and decreased with decreasing grain size.

The Coffin-Manson[5,6] relationship may be used to analyze the effect of grain size on LCF life:

$$\frac{\Delta\varepsilon_p}{2} = \varepsilon'_f(2N_f)^{-c} \qquad (1)$$

where,

$\frac{\Delta\varepsilon_p}{2}$ is the plastic strain amplitude,

ε'_f is the fatigue ductility coefficient,

N_f is the number of cycles before failure,

and

c is the fatigue ductility exponent.

Often ε'_f is considered to be approximately equal to the monotonic true fracture strain, ε_f[5]. Equation 1 shows that any factor (e.g., grain

size) which will affect the ductility, and consequently ε'_f, will change the LCF life. This qualitative argument is supported by the results of Thompson and Backofen[24], who reported a marked grain size dependence of fatigue life in copper and aluminum for lives shorter than 10^5 cycles. For brass, as might be expected, an even larger grain size effect was exhibited in the LCF range.

Laird and Feltner[32] attributed grain size effects on LCF to the nucleation and growth of stage I cracks at grain boundaries. As the severity of surface deformation increases during a fatigue test, folding occurs at grain boundaries to accommodate differences in strain between adjacent grains[25]. The folds become more severe, until stage I cracks are initiated. The increased stress intensity at the tip of the stage I crack gives rise to the grain size dependence of LCF. Unlike the case of high cycle fatigue, dislocation cell structure does not inhibit stage I crack growth. Grain boundaries become the dominant factor in controlling the severity of folding and resultant stage I cracking. A similar argument was offered by Feltner and Beardmore[33] who proposed that slip offsets and resultant stresses developed at grain boundaries are smaller in fine-grained materials (regardless of slip mode). Thus, the occurrence of crack initiation is delayed and LCF life is increased for smaller grain sizes. However, the authors cited data to show that very large reductions in grain size are necessary to obtain rather limited improvements in LCF life. They observed that achievement of increases in the cohesive strength of grain boundaries would also be beneficial to LCF resistance.

Deviations in the Coffin-Manson Relation for Al Alloys

The following relationship between plastic strain range ($\Delta\varepsilon_p$) and fatigue life (N_f) was first proposed by Coffin[5] for low cycle fatigue:

$$\Delta\varepsilon_p = CN_f^{-1/2} \tag{2}$$

When plotted on a log-log basis, $\Delta\varepsilon_p$ versus N_f yields a straight line with a slope of -1/2. Coffin suggested also that the value of C correlated well with the tensile fracture strain (ε_f). When tested experimentally, Coffin's relation applied well to the fatigue behavior of most materials.[5,10]. However, data for Al - 3.64 Cu[34], Al - 5 Mg[34], and two commercial aluminum alloys[10], 24S-T and 75S-T, showed marked deviations from the straight line relation. At low values of $\Delta\varepsilon_p$, fatigue lives were considerably shorter than predicted by Equation (2). Coffin[10] offered the explanation that strain-localizing effects, such as surface defects, environment, or precipitate structures become relatively more important as $\Delta\varepsilon_p$ is lowered. These effects could lead to large localized strain concentrations, causing premature crack initiation and failure. However, no experimental work was done to check this hypothesis.

Manson[6] subsequently questioned the universality of the exponent, -1/2, in Coffin's relationship. He argued that LCF data would better be represented by the use of an empirical material constant, z, as the exponent in Equation (2). Using Manson's modification of Coffin's relationship, z for most materials was determined to be closer to -0.6 than -0.5[6]. But despite the new method of analysis, LCF data for 2024-T4 and 7075-T6 showed marked deviations from linearity at low $\Delta\varepsilon_p$ values.

Endo and Morrow[35] also found that LCF data for 2024-T4 and 7075-T6 were not adequately described by the Coffin-Manson relationship in the low plastic strain range. The only explanation offered was the possible influence of differences in strain measuring techniques at high and low $\Delta\varepsilon_p$. However, the scatter in their data was minimal and no deviations in the straight line relationship were observed in their LCF results for steels and a titanium alloy.

Coffin[9] explains the failure of the $\Delta\varepsilon_p - N_f$ law most commonly observed in brittle materials by a change in the mode of crack propagation with $\Delta\varepsilon_p$. At high strain amplitudes, predominantly ductile, transgranular crack propagation and fracture predominates. As $\Delta\varepsilon_p$ is lowered, crack propagation becomes more brittle due to localized microstructural and environmental effects. According to Coffin, the LCF plot should be divided into two straight line portions, with a break at 50-100 cycles, corresponding to the change in crack propagation mode. The high strain portion of the curve should have a slope of -0.5 and extrapolate to the value of ε_f at $N = 1/4$[5]. The slope of the low strain amplitude portion of the curve would be more negative than -0.5, the exact value depending upon the effects causing the deviation. Most of Coffin's data was derived from LCF studies of steels at elevated temperature but when the two-slope correlation was applied to the data of Manson and Hirschberg[6] for 2024-T4 and 7075-T6, a reasonably good fit was achieved.

Tomkins[8] derived the Coffin-Manson relationship from an analysis of the crack propagation process to obtain:

$$\Delta\varepsilon_p = C(N_f)^{\frac{-1}{2m'+1}} \qquad (3)$$

Thus the slope of the Coffin-Manson plot is inversely proportional to the capacity of the material to cyclically harden. Equation (3) provided a good approximation to the LCF data for reasonably ductile materials[8]. Tomkins tested several materials (no aluminum alloys) whose LCF data failed to follow the Coffin-Manson relation. The difference in the fatigue ductility exponent as a function of strain amplitude was correlated to a change in slope (n') of the logarithmic cyclic stress-strain curve. A later modification of Tomkins'[36] theory cited evidence of secondary cracking ahead of the fatigue crack to explain the deviations from the Coffin-Manson relation observed in the LCF data. Calabrese and Laird[37] applied Tomkins' theory[8] in an effort to predict the LCF life of Al-4Cu aged to give various precipitate structures. The failure of the Coffin-Manson relationship shown by their data at low plastic strain amplitudes was not explained by the investigators who concluded only that the Tomkins' model gave a "conservative, but reasonable" estimate of LCF life in their study.

Other workers have explained such behavior from the standpoint of microstructural effects on deformation mode and subsequent crack initiation. Saxena and Antolovich[7] plotted the fatigue life and plastic work per cycle versus N_f for high- and low-SFE Cu - Al alloys. A break found in these plots for the low-SFE alloy was attributed to the difficulty of cross slip in this alloy. The coincidence of the breaks in the plastic work $-N_f$ and $\Delta\varepsilon_p/2 - N_f$ plots indicates that the non-linearity must be related to cyclic deformation prior to crack initiation. Sanders and Starke[4] observed a break in the Coffin-Manson plot of a 7050 alloy

aged to produce incoherent η precipitates. Through a TEM study, the LCF results were correlated to a change in deformation mode with strain amplitude. At large values of $\Delta\varepsilon_p/2$ (>1%), dislocation cell formation occurred most readily, while dislocation banding predominated at lower $\Delta\varepsilon_p/2$. The LCF results of Selines[3] for 2024 and 7075 show marked deviations from the Coffin-Manson relation at strain amplitudes below 0.4 per cent. By testing samples in an extremely inert organic fluid, possible environmental causes of the breaks in the curves were eliminated. (Other results[41] for LCF of 2024-T4 in air and vacuum showed no effect of environment on the fatigue life.) Selines offers an explanation similar to the original hypothesis of Coffin[10]: that the presence of localized strain concentrations, causing parts of the specimen to undergo larger plastic strain amplitudes than macroscopically measured, results in a deviation from the straight-line relationship predicted by the Coffin-Manson relationship. A recent LCF study by Sanders et al.[39] at Alcoa showed a number of aluminum alloys to exhibit the typical break in the Coffin-Manson relation at low $\Delta\varepsilon_p/2$. TEM of fatigued samples revealed a marked tendency toward strain localization at the low strain amplitudes.

CHAPTER III

EXPERIMENTAL PROCEDURES

The alloys studied in this research were prepared at the Alcoa Technical Center, Alcoa Center, Pennsylvania. The exact series of thermal and mechanical treatments used in the preparation of the Al-Zn-Mg-Zr alloy is considered proprietary by Alcoa and cannot be described here. The alloy was received in plate form with a nominal thickness of 0.58 cm. The Al-Zn-Mg alloy plate was hot-rolled from the cast ingot at 750°F (399°C) to a nominal thickness of 0.43 cm. The chemical compositions in weight percent of the two alloys are shown in Table 1 along with that of a 7050 alloy for comparison.

A section of the Al-Zn-Mg-Zr plate was solutionized for 1 1/2 hours at 480°C and quenched in ice brine; this will be designated as the standard method of heat treatment. Samples were cut, mounted, and polished for metallographic examination of the three principal sections of the plate. Transmission electron microscopy (TEM) was also used to characterize the as-received and solutionized structures of the plate. Foils were dimpled and electropolished using standard techniques. Microscopy was done using a Siemens Elmiskop 1A operating at 125 KV.

Samples of both alloys were cold-rolled, with an intermediate anneal, to a thickness of 0.76 mm, approximately $1/\mu$, where μ is the x-ray absorption coefficient for molybdenum radiation. The rolled strips were heat treated in the standard manner and immediately (within 30

Table 1. Composition of the Aluminum Alloys

	Si	Fe	Cu	Mn	Mg	Cr	Zn	Ti	Be	Zr
Al-Zn-Mg	0.00	0.00	0.00	0.00	2.20	0.00	6.17	0.00	0.00	0.00
Al-Zn-Mg-Zr	0.05	0.04	0.01	0.00	2.08	0.00	6.45	0.02	0.00	0.11
7050	0.06	0.08	2.55	0.01	2.21	0.01	6.31	0.02	0.001	0.10

seconds) transferred to a constant temperature oil bath for aging at 120°C or 150°C. The strips were degreased and mounted on a Kratky camera for examination by XSAS. A high-intensity molybdenum x-ray source, operating at 50 KV and 20 ma was used. Entrance and exit slit heights of 80 and 160 μm respectively were employed. The Guinier approximation was used in analyzing the raw data to determine the particle radius of gyration[40].

Flat-plate tensile specimens were prepared from the as-received material in accordance with ASTM specifications[41]. The specimens were four inches in length with a gage length of approximately 1 inch. The dimensions of the gage section were 0.25 inches by the plate thickness. The specimens were cut with the gage section parallel to the rolling direction. The tensile samples were heat treated by the standard method and immediately aged. Before testing, the two flat sides of each specimen were ground and polished to a 1μ finish to facilitate observations of surface deformation. The specimens were strained to fracture in uniaxial tension on an Instron testing machine at a strain rate of approximately 6.6×10^{-4}/sec.

Fatigue samples of the Al-Zn-Mg-Zr alloy were machined with the gage section parallel to the rolling direction of the plate. The specimens were cylindrical with a gage section approximately 5 mm long by 3 mm diameter. The machined samples were heat treated in the standard manner and immediately aged. The surfaces of the aged specimens were hand polished with polishing cloths impregnated with 6μ and 1μ diamond paste. The specimens were finally electropolished in a 25% HNO_3-methanol solu-

tion. Fully-reversed push-pull low cycle fatigue tests were carried out on an Instron testing machine in a dry argon atmosphere. The strain was controlled by a 10 mm Instron extensometer clamped to posts rigidly attached to the sample grips. A Wood's metal reservoir was used to insure proper alignment of the sample with respect to the loading axis. The Wood's metal was remelted and the extensometer recalibrated before each test. All tests were begun at a total strain rate of approximately 3.3 x 10^{-4}/sec. For longer tests, specimens were cycled to saturation (at least 200 cycles) at 3.3 x 10^{-4}/sec., then cycled to failure at 6.6 x 10^{-4}/sec.

The fracture surfaces of selected fatigue and tensile specimens were examined on a Cambridge Stereoscan equipped with a nondispersive x-ray detector. Thin foils of fatigued specimens taken from sections 1-3mm below the fracture surface were prepared and examined by TEM. Sections of fractured tensile and fatigue specimens were polished and etched for examination by optical microscopy.

CHAPTER IV

EXPERIMENTAL RESULTS

Solution treatment of the Al-Zn-Mg-Zr alloy for 1 1/2 hours at 480°C produced a partially recrystallized microstructure with mean grain dimensions of approximately 0.03 mm x 0.05 mm x 0.10mm. The as-received and solutionized microstructures are shown in Figure 1. The large variation in grain dimensions and incomplete recrystallization discouraged any attempt to make a precise grain size measurement. The grains were roughly pancake-shaped and severely elongated in the rolling direction. A small volume fraction of intermetallic particles was found strung out in the rolling direction of the plate. These particles are probably Al-Fe-Si compounds[1] resulting from the presence of 0.04% Fe and 0.05% Si as impurities.

Examination by TEM showed that a large degree of subgrain coalescence occurred during solutionizing. The fine dislocation cell structure introduced during hot working of the alloy plate coalesced into larger subgrains during the heat treatment at 480°C as shown in Figure 2. The solutionized microstructure is very non-uniform in size and shape and is free from most of the precipitates and dislocation debris found in the as-received plate.

The effect of a series of double aging treatments on the precipitate size was investigated by x-ray small angle scattering (XSAS). Samples were aged at 120°C for varying times, then for 12 hours at 150°C.

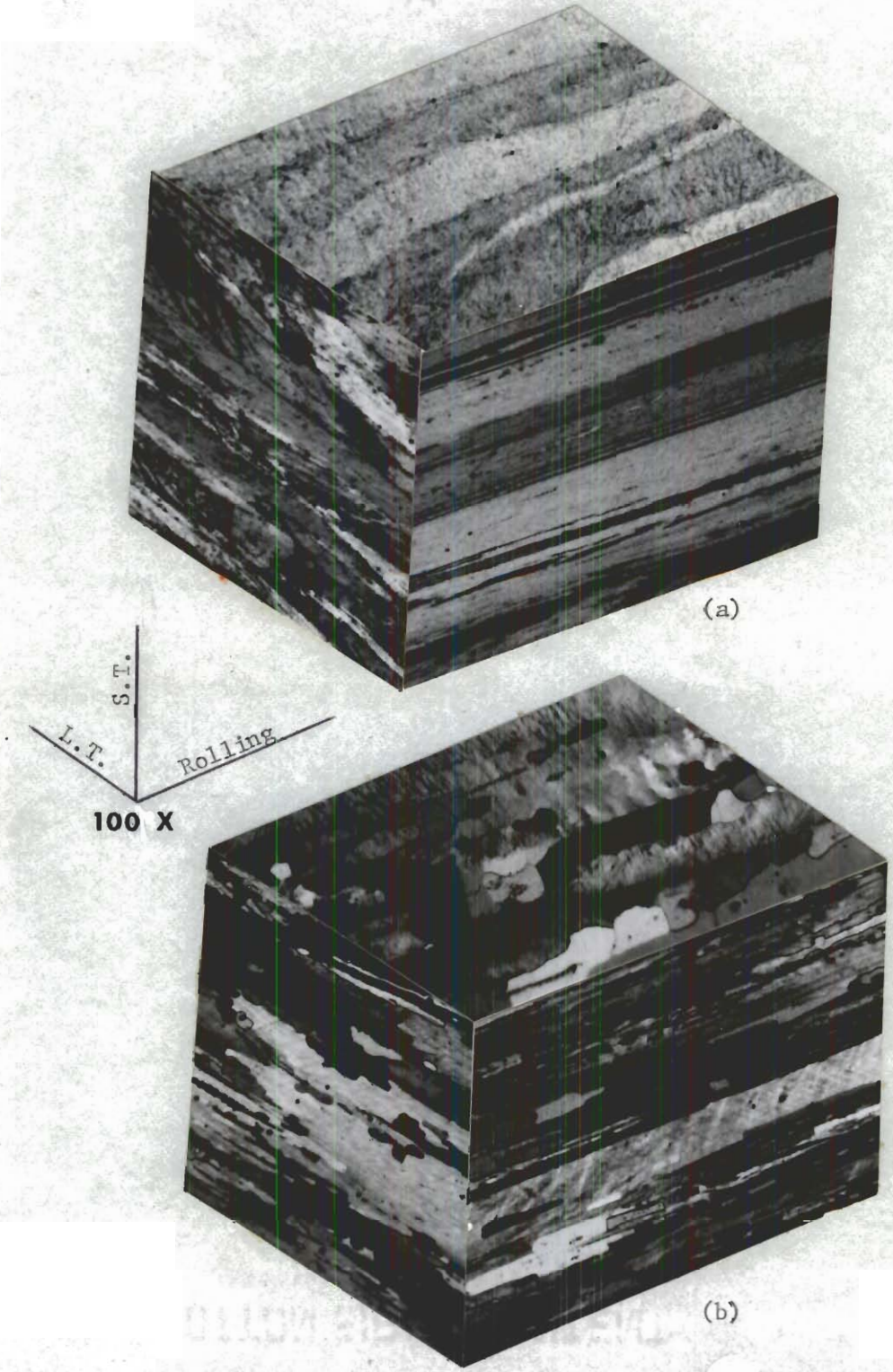

Figure 1. Microstructure of Al-Zn-Mg-Zr Plate: **(a)** as-received, and (b) after solutionizing at 480°C for 1 1/2 hours. Anodized, 4% HBF_4.

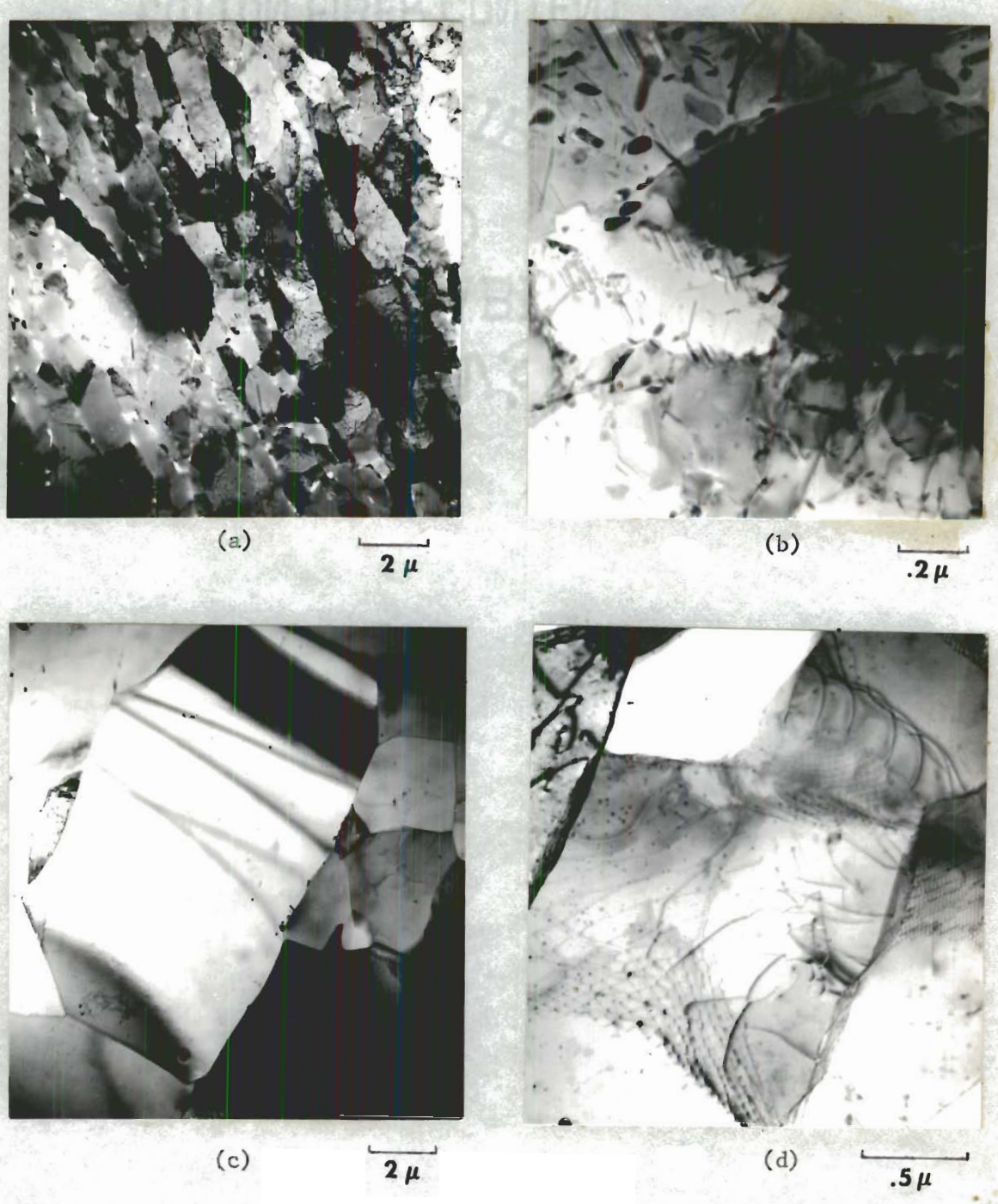

Figure 2. Subgrain Structure of the Al-Zn-Mg-Zr Plate: (a) and (b) as received, (c) and (d) after solutionizing at 480°C for 1 1/2 hours.

The radii of gyration (R_g) calculated from the Guinier approximation are given in Table 2. Also included in Table 2 are data from the work of Sanders and Starke[4] who studied precipitation kinetics in a similar Al-Zn-Mg alloy and a commercial 7050 (Al-Zn-Mg-Cu-Zr) alloy.

It is evident from this data that the addition of 0.1 percent zirconium did not significantly affect precipitation in this alloy system. This is expected since the zirconium is precipitated as stable Al_3Zr approximately 0.1 in diameter[1] after homogenization and should not be altered during subsequent aging treatments. Figure 3 shows the effect of aging at 120°C and 150°C on R_G of Al-Zn-Mg and 7050[4]. Discounting any possible effects of the zirconium addition on precipitation in the system, the data for Al-Zn-Mg may be used to describe the aging of the Al-Zn-Mg-Zr alloy. The results in Table 2 show that a pre-aging time of 2 hours at 120°C was sufficient to provide nuclei stable at the higher aging temperature, 150°C. Aging these pre-aged samples for 12 hours at 150°C produced a microstructure of mostly η'[40], and probably some $\eta(MgZn_2)$, having $R_G = 30\text{Å}$. The DA 2424 aging treatment produced a similar microstructure with a larger ($R_G = 47$ Å) precipitate size. Examination of selected area diffraction (SAD) patterns taken during a TEM study of double-aged samples disclosed the presence of diffraction spots associated with the presence of these precipitates. Aging for 24 hours at 150°C produced a precipitate structure consisting of large, incoherent η particles with $R_G = 71$ A[4].

Tensile tests were conducted on double aged specimens of both alloys to select appropriate aging treatments for low cycle fatigue

Table 2. Effect of Aging Treatment on Precipitate Size in Al-Zn-Mg-Zr, Al-Zn-Mg, and 7050

Aging treatment Designation	Aging Time (hrs) 120°C	150°C	Guinier Radius (Å) Al-Zn-Mg-Zr	Al-Zn-Mg*	7050*
DA212	2	12	29	-	-
DA412	4	12	29	30	-
DA612	6	12	31	-	-
DA1212	12	12	30	-	-
4@120	4	-	-	25	23
24@150	-	24	-	71	80
DA2424	24	24	-	47	45

* from work of Sanders and Starke[4]

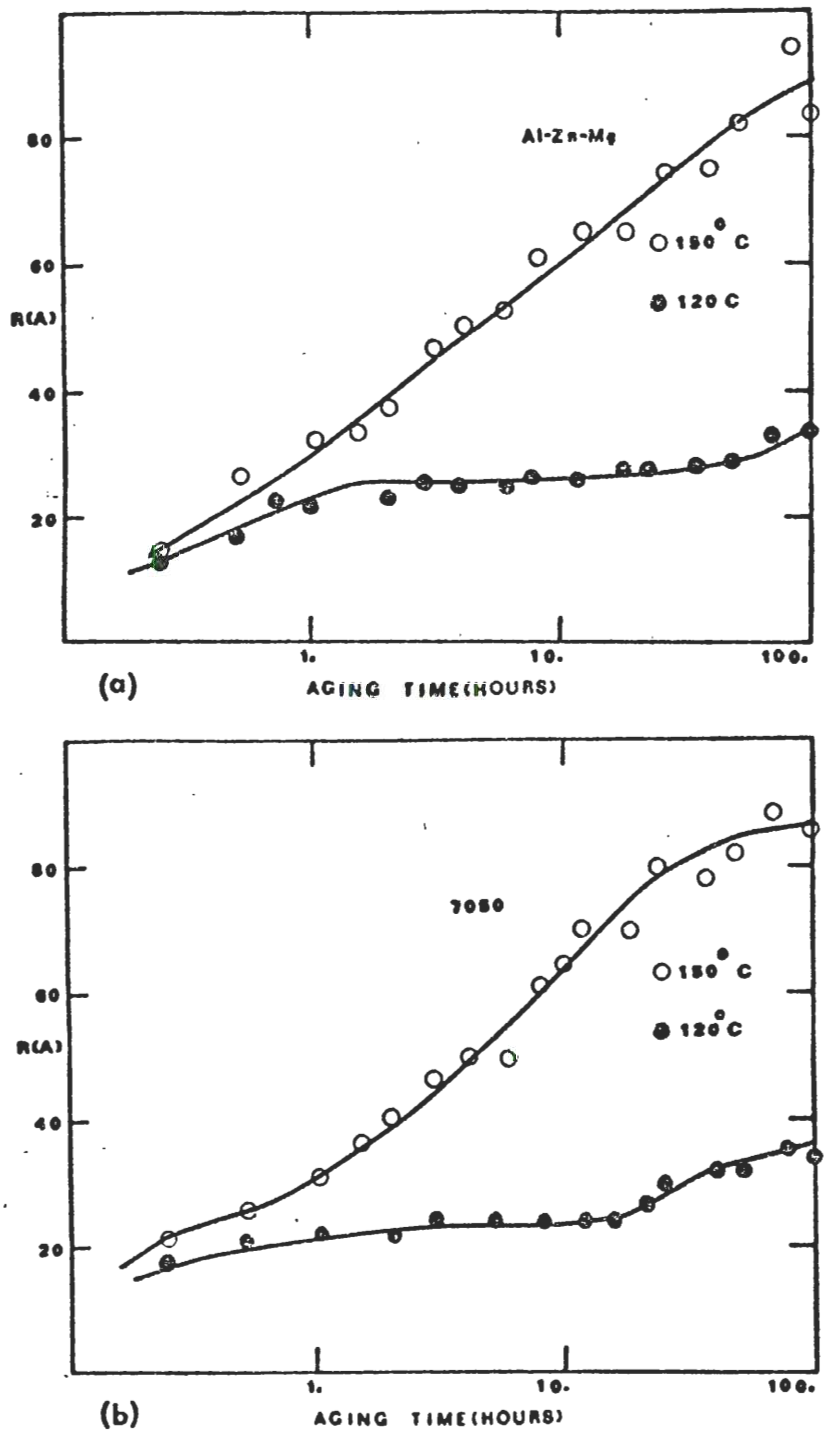

Figure 3. Variation of Guinier Radius with Aging Time: (a) Al-Zn-Mg, and (b) 7050. (from the work of Sanders and Starke[4]).

studies. The results of these and subsequent tests are shown in Table 3. All values reported are averages of results for two specimens. Differences in the data averaged to give the results in Table 3 were less than 5 percent for the strength data and less than 10 percent for the elongation data.

The data in Table 3 show that the addition of ~0.1% zirconium to the Al-Zn-Mg alloy produced increases of ~6 percent in the .2% yield and the ultimate tensile strengths for the double-aged samples. Increases in strength for the 4@120 and 24@150 samples were somewhat greater. The most marked result, however, was the increase in ductility obtained by the grain size reduction. Five of the aging treatments were selected and LCF data were obtained for the Al-Zn-Mg-Zr alloy.

The results of the low cycle fatigue tests are shown in Figures 4 through 8 plotted as:

(a) cyclic stress amplitude versus number of cycles,

(b) log $\Delta\varepsilon_p/2$ versus log $2N_f$ (Coffin-Manson relationship), and

(c) logarithmic monotonic and cyclic stress-strain curves.

The theoretical basis for treating the data in this manner is discussed by Sandor[42]. For each Coffin-Manson plot and cyclic stress-strain curve, the best straight line fit to the data was obtained by a linear regression analysis. An extrapolation of the best fit was made for each Coffin-Manson plot to determine the value of $\Delta\varepsilon_p$ at $2N_f = 1/2$. This point, known as the fatigue ductility coefficient, ε_f', is shown on each plot along with the value of ε_f, the true monotonic strain to fracture. The LCF results were compared with the data of Sanders and Starke[4] for Al-Zn-Mg and 7050. Examination of the LCF data, Figures 5a-8a, shows

Table 3. Preliminary Tensile Data for Al-Zn-Mg-Zr and Al-Zn-Mg

Aging Treatment (See Table 2)	Al-Zn-Mg-Zr			Al-Zn-Mg		
	.2% Yield (MN/m^2)	UTS (MN/m^2)	elongation* (%)	.2% Yield (MN/m^2)	UTS (MN/m^2)	elongation* (%)
DA212	445	469	13.8	419	429	1.5
DA412	440	465	14.8	424	433	1.2
DA612	443	473	14.6	427	436	1.1
DA1212	442	470	13.6	421	429	1.2
4@120	368	441	18.8	303	369	10.7
24@150	378	412	15.4	325	361	3.5
DA2424	415	447	15.2	406	418	1.3

* measured in 1 inch gage length.

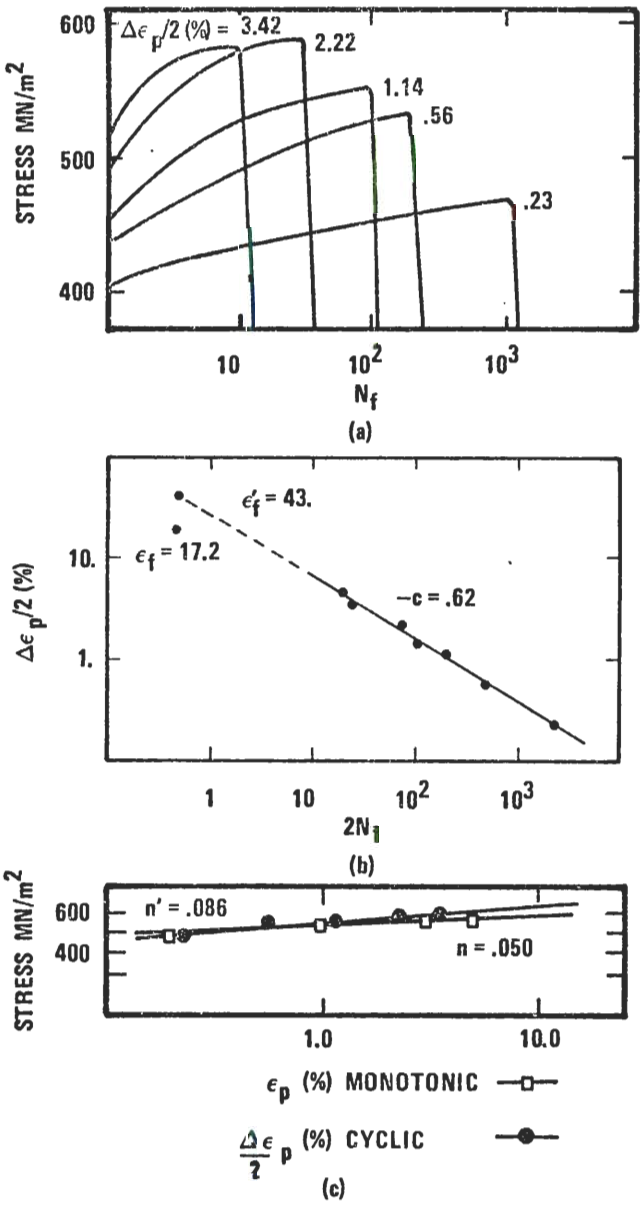

Figure 4. Low Cycle Fatigue Behavior of Al-Zn-Mg-Zr Aged 4 Hours at 120°C (4@120): (a) stress amplitude versus cycles, (b) Coffin-Manson plot, and (c) cyclic and monotonic stress-strain curves.

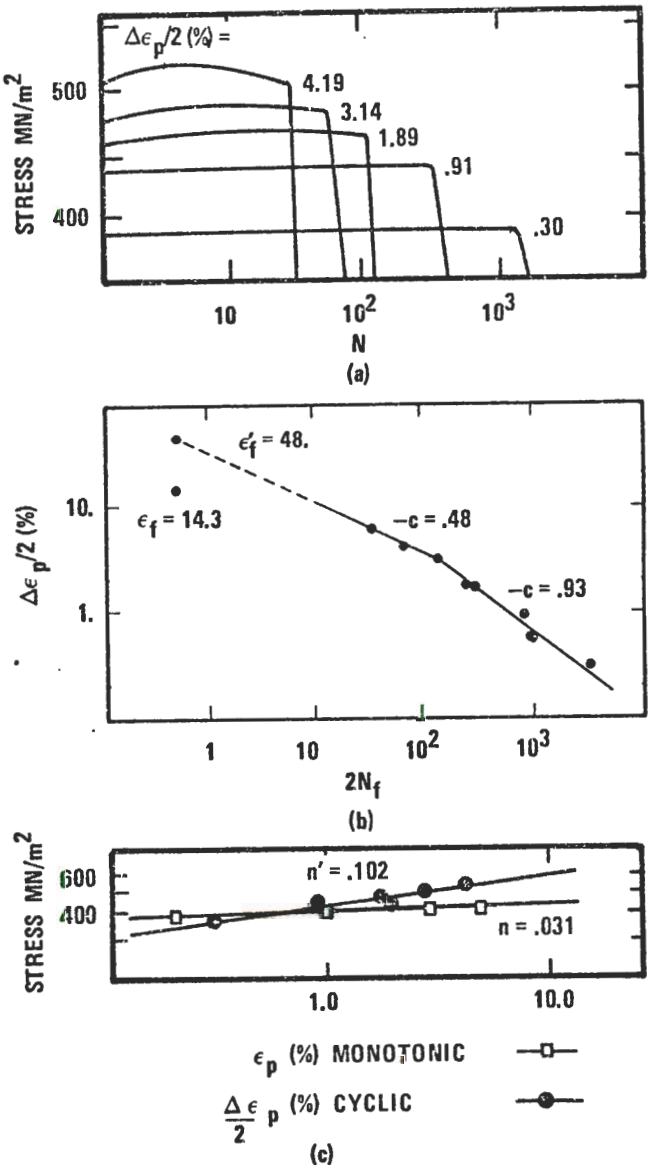

Figure 5. Low Cycle Fatigue Behavior of Al-Zn-Mg-Zr Aged 24 Hours at 150°C (24@150): (a) stress amplitude versus cycles (b) Coffin-Manson plot and (c) cyclic and monotonic stress-strain curves.

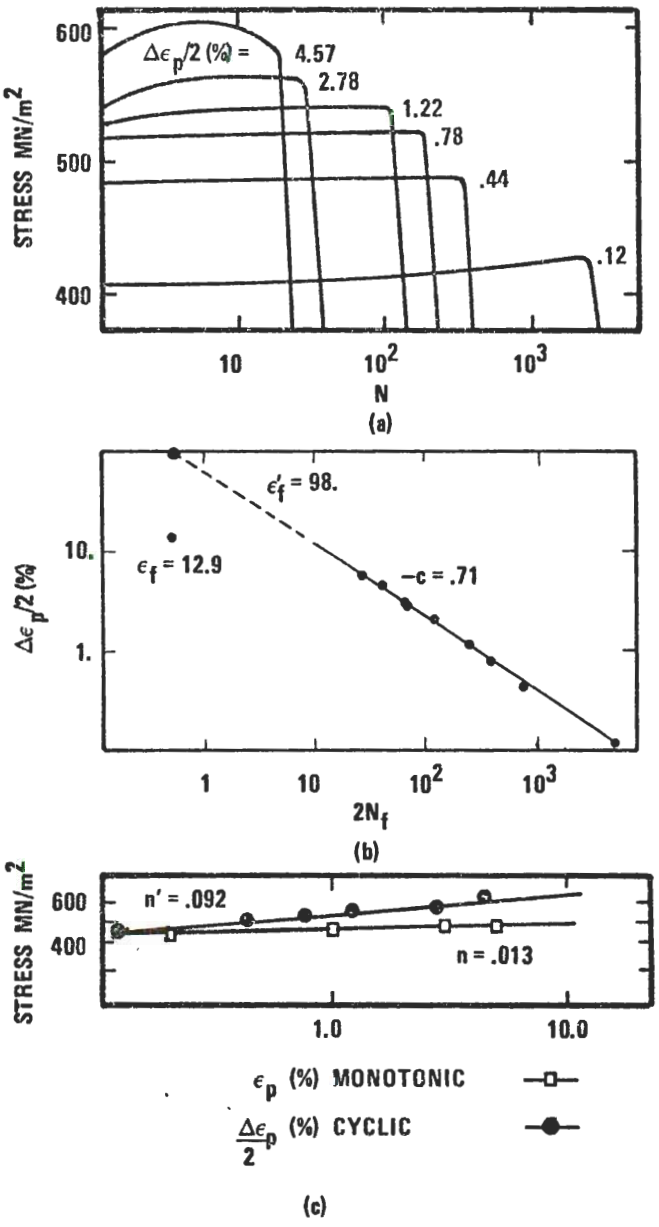

Figure 6. Low Cycle Fatigue Behavior of Double-Aged Al-Zn-Mg-Zr, 2 Hours at 120°C Followed by 12 Hours at 150°C (DA212): (a) stress amplitude versus cycles, (b) Coffin-Manson plot, and (c) cyclic and monotonic stress-strain curves.

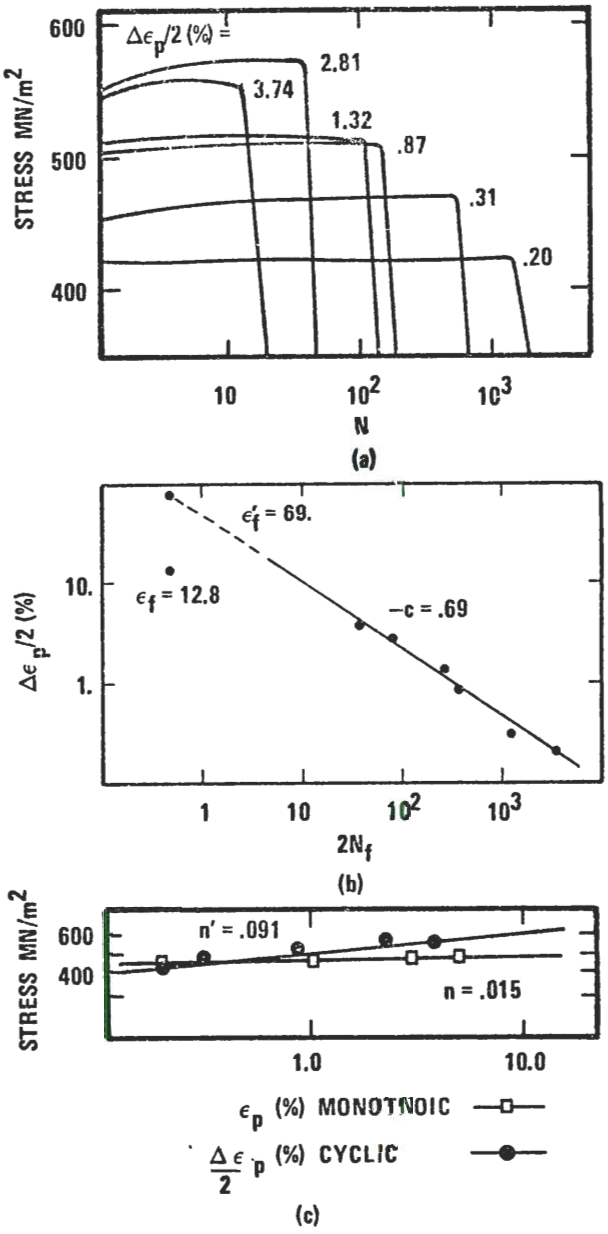

Figure 7. Low Cycle Fatigue Behavior of Double-Aged Al-Zn-Mg-Zr, 12 Hours at 120°C Followed by 12 Hours at 150°C (DA1212): (a) stress amplitude versus cycles, (b) Coffin-Manson plot, and (c) cyclic and monotonic stress-strain curves.

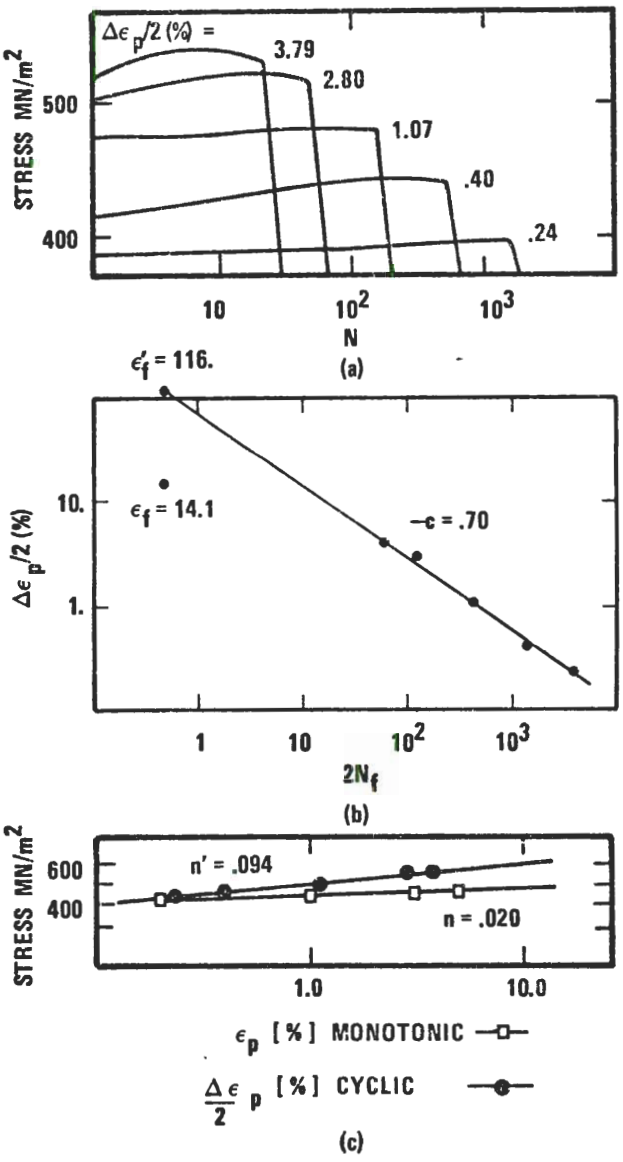

Figure 8. Low Cycle Fatigue Behavior of Double-Aged Al-Zn-Mg-Zr, 24 Hours at 120°C Followed by 24 Hours at 150°C (DA2424): (a) stress amplitude versus cycles, (b) Coffin-Manson plot, and (c) cyclic and monotonic stress-strain curves.

that the double-aged and 24@150 samples tended to saturate immediately or cyclically harden slightly. In many instances the saturation stress amplitude was reached after only a few cycles. The 4@120 samples, however, showed a large degree of cyclic hardening up until the point of crack initiation and saturation never occurred, Figure 4a. For this reason, the logarithmic cyclic stress-strain curve for this aging treatment was plotted using the value of the stress amplitude at 1/2 N_f. It has been suggested previously that, for LCF tests, $\varepsilon_f' = \varepsilon_f$. The lack of correspondence of these two values in the present study is obvious from examination of the Coffin-Manson plots and will be considered later in more detail. The slope of the Coffin-Manson curves, c, ranged between -.62 and -.70 for LCF data of the aging treatments studied, with the exception of the 24@150 condition. A break was noted at $N_f \simeq 75$ cycles in the Coffin-Manson plot for this aging treatment. Samples cycled at low plastic strain amplitude exhibited much shorter lives than would be predicted by extrapolation from the high strain amplitude portion of the plot. Table 4 contains a complete tabulation of the tensile and LCF parameters for the five aging treatments studied. Also included are data for Al-Zn-Mg and a 7050 alloy[4]. Appendix A contains the complete data for each individual LCF test.

Optical microscopy revealed the presence of slip markings on polished surfaces of tensile specimens as shown in Figure 9. Coarse slip lines were observed on the surfaces of Al-Zn-Mg samples, Figures 9a and 9b. Offsets at the grain boundaries were evident in these samples, being most severe for the 4@120 aging treatment. Evidence of transgranular cracking was observed in the 4@120 samples shown in Figure 9c. Slip lines

Table 4. Tensile and Cyclic Properties of Al-Zn-Mg-Zr, Al-Zn-Mg and 7050

Sample	TENSILE												CYCLIC								
	Yield (MN/m^2)			UTS (MN/m^2)			n			ϵ_f (%)			-C			n'			ϵ_f' (%)		
	Al-Zn Mg	Al-Zn Mg-Zr	7050	Al-Zn Mg	Al-Zn Mg-Zr	7050	Al-Zn Mg	Al-Zn Mg-Zr	7050	Al-Zn Mg	Al-Zn Mg-Zr	7050	Al-Zn Mg	Al-Zn Mg-Zr	7050	Al-Zn Mg	Al-Zn Mg-Zr	7050	Al-Zn Mg	Al-Zn Mg-Zr	7050
4@120	303	368	490	369	441	-	.055	.050	.065	10.2	17.2	20	.50	.62	.61	.045	.086	.12	14.1	43	29.0
DA212	419	445	-	429	469	-	-	.013	-	1.5	12.9	-	-	.71	-	-	.092	-	-	98	-
DA1212	421	442	-	429	470	-	-	.015	-	1.2	12.8	-	-	.69	-	-	.091	-	-	69	-
24@150	325	378	519	361	412	-	.05	.030	.080	3.4	14.3	13	.46	.48 .92	.45 .85	.05	.102	.11	18.0	48 632	23.2 172
DA2424	406	415	568	418	447	-	-	.020	.015	1.3	14.1	11	-	0.70	.67	-	.094	.015	-	116	41.4

ε_f = 1.2% (a) 35X

ε_f = 10.2% (b) 35X

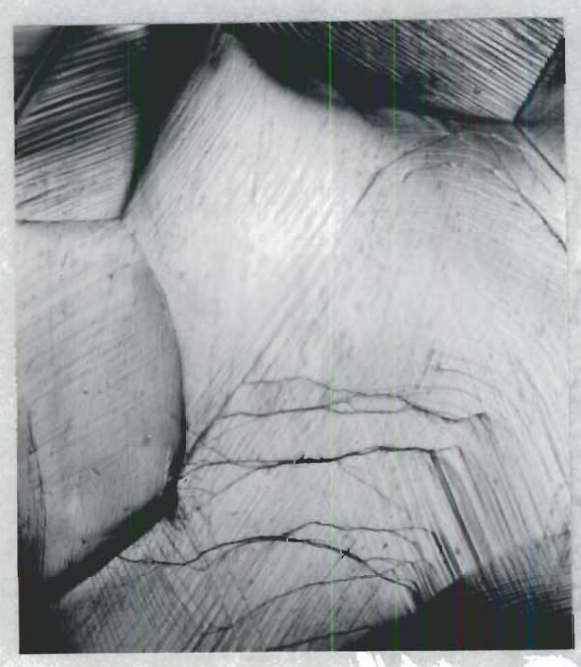

ε_f = 10.2% (c) 75X

ε_f =14.3% (d) 75X

Figure 9. Observations of Slip on Polished Surfaces of Tensile Samples: (a) Al-Zn-Mg, DA1212, (b) and (c) Al-Zn-Mg, 4@120, and (d) Al-Zn-Mg-Zr, 24@150.

were observed less frequently on polished surfaces of Al-Zn-Mg-Zr tensile specimens. A typical surface is shown in Figure 9d.

Additional evidence of localized slip was found by sectioning, polishing, and etching Al-Zn-Mg tensile and fatigue specimens. Figure 10 shows slip markings revealed by metallographic examination of fractured 24@150 and 4@120 Al-Zn-Mg tensile specimens. Transgranular cracking, evident in the 4@120 sample, was not observed in the 24@150 specimen, even after additional etching. An etched longitudinal section of an Al-Zn-Mg fatigue sample used in a previous work[4] was examined, Figure 10c. The slip markings are similar to those of the 24@150 tensile specimen shown in Figure 10a. However, the fatigued specimen showed an increased tendency to develop stress concentrations in areas adjacent to intersection points of three grains. Similarly etched sections of Al-Zn-Mg-Zr tensile and fatigue specimens revealed localized slip markings in some of the larger grains, but their presence was much less frequent than observed in sections of Al-Zn-Mg samples.

Examination of tensile fracture surfaces showed that intergranular fracture occurred for all aging conditions of the Al-Zn-Mg alloy, Figure 11a. Dimpled features characteristic of ductile failure were noted for tensile fracture of the Al-Zn-Mg-Zr alloy as shown in Figure 11b. Transmission electron microscopy showed pronounced dislocation banding in thin foils of fractured double-aged Al-Zn-Mg tensile specimens. Examination of similarly aged Al-Zn-Mg-Zr foils showed a much more homogeneous dislocation distribution with a slight tendency toward dislocation banding. Typical micrographs are shown in Figure 12.

ε_f = 3.4% (a) 35X

ε_f = 10.2% (b) 35X

(c) 100X

Figure 10. Observations of Slip Traces in Metallographic Sections of Al-Zn-Mg Tensile and Fatigue Specimens: (a) transverse section 24@150 tensile, (b) transverse section 4@120 tensile, and (c) longitudinal section 24@150 fatigue, N_f = 141.

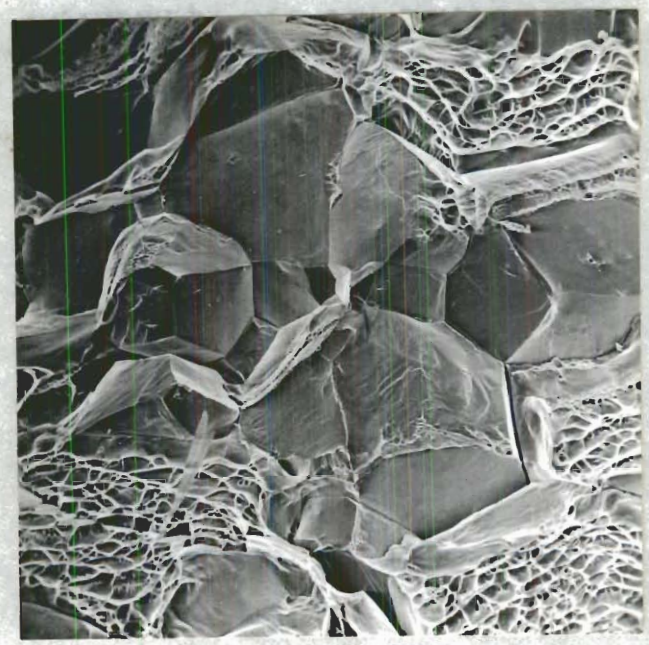

(a)

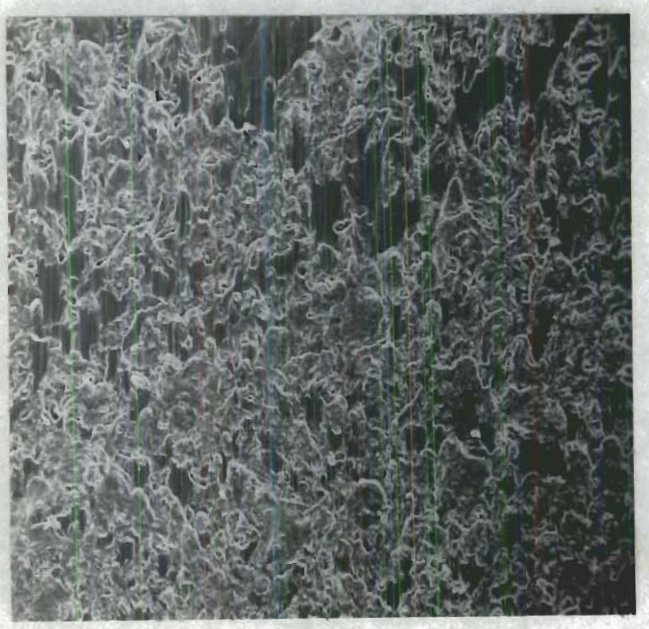

(b)

Figure 11. Observations of Tensile Fracture in the Two Alloys: (a) Al-Zn-Mg, DA1212, ε_f = 1.2%, 74X, and (b) overload area of Al-Zn-Mg-Zr, 24@150 fatigue specimen, $\Delta\varepsilon_p/2$ = 0.47% 112X.

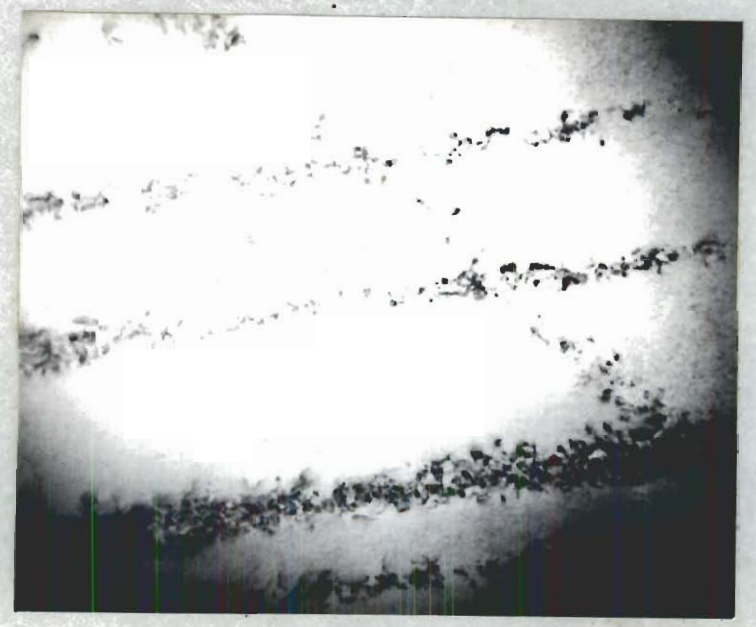

(a) 1μ

(b) 1μ

(c) 1μ

Figure 12. Transmission Electron Micrographs of Transverse Sections of Fractured DA1212 Tensile Samples: (a) Al-Zn-Mg, ε_f = 1.2%, (b) and (c) Al-Zn-Mg-Zr, ε_f = 12.8%.

Selected scanning micrographs of fractured fatigue samples are shown in Figure 13. The fracture surfaces of Al-Zn-Mg samples used in Sanders' work were characterized by a transgranular ring of fatigue damage surrounding a large region of intergranular overload tensile fracture. Striations, characteristic of stage II crack propagation, were noted in the fatigued regions. Examination of Al-Zn-Mg-Zr fatigue samples revealed that fracture occurred primarily at 45 degrees to the stress axis. This fracture is shown in Figure 13b. Regions of ductile fatigue striations were observed on fracture surfaces of most fatigue specimens, and were accompanied in some areas by the presence of secondary cracking, Figure 14. Few fatigue striations were observed on fracture surfaces of Al-Zn-Mg-Zr specimens fatigued at high plastic strain amplitudes where a proportionately larger area of ductile tensile overload fracture was noted.

An optical examination of Al-Zn-Mg-Zr fatigue specimens showed that slip markings were consistently parallel as if deformation were confined to a single slip system. Intergranular cracks in the longitudinal direction were occasionally observed adjacent to highly deformed grains near the fracture surfaces of some specimens. Samples cycled at high strain amplitudes showed more pronounced slip markings accompanied by increased intergranular cracking. These observations are possibly analogous to the intergranular cracks observed in a metallographic examination of a sectioned tensile specimen, Figure 15. No significant differences were noted in surface deformation of double-aged and 24@150 fatigue samples. The 4@120 samples showed more severe slip markings than the other aging treatments investigated for a given strain amplitude. Transgranular

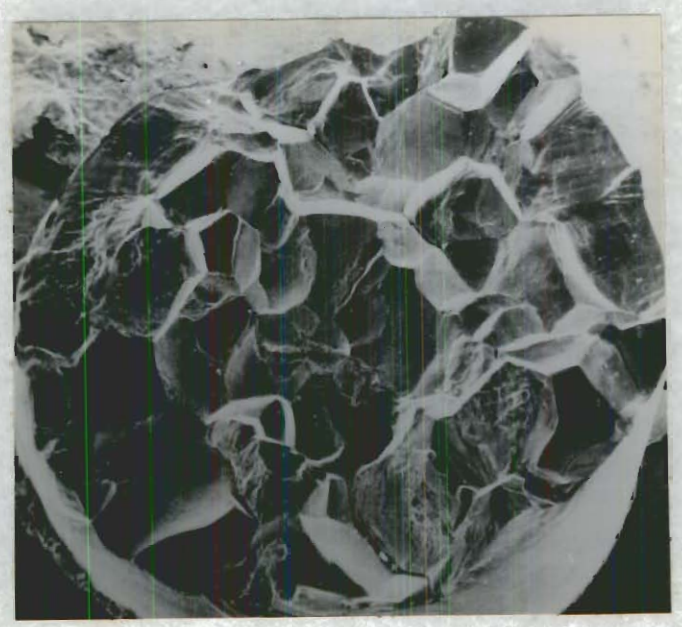

(a)

(b)

Figure 13. Macroscopic Scanning Fractographs of Typical 24@150 Fatigue Fracture Surfaces: (a) Al-Zn-Mg, $\Delta\varepsilon_p/2$ = 1.10%, 33X, and (b) Al-Zn-Mg-Zr, $\Delta\varepsilon_p/2$ = 0.47%, 30X.

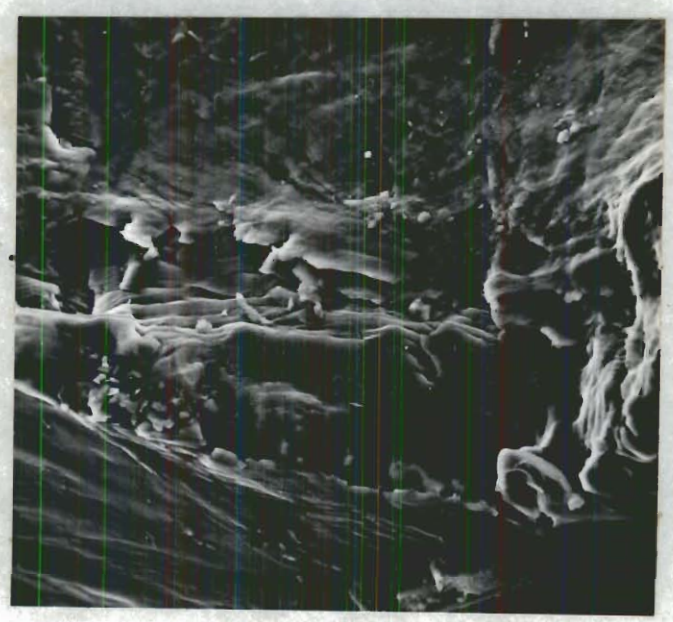

(a)

(b)

Figure 14. Scanning Micrographs Showing Typical Fatigue Striations and Secondary Cracking in Al-Zn-Mg-Zr, 24@150, Fatigue Specimens: (a) $\Delta\varepsilon_p/2$ = 3.17%, 680X, and (b) $\Delta\varepsilon_p/2$ = 0.47%, 590X.

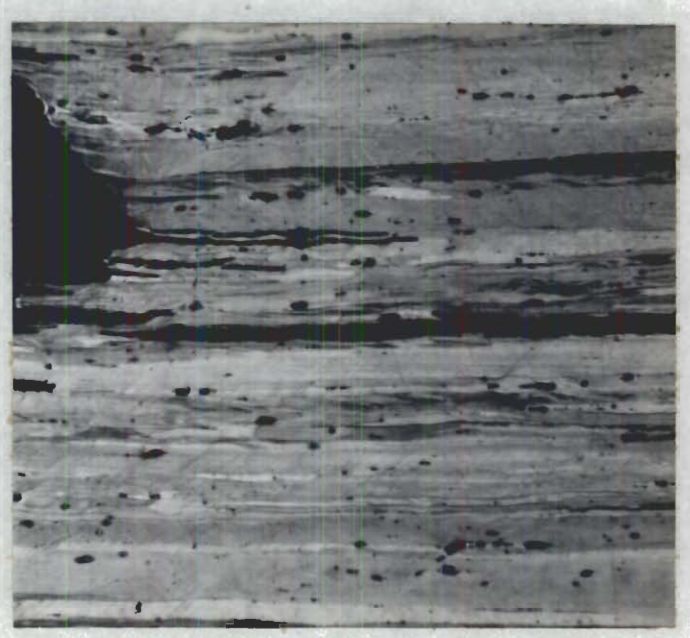

Figure 15. Polished and Anodized Longitudinal Section of Al-Zn-Mg-Zr DA2424 Tensile Sample Showing Fracture Surface and Associated Intergranular Cracks, 100X.

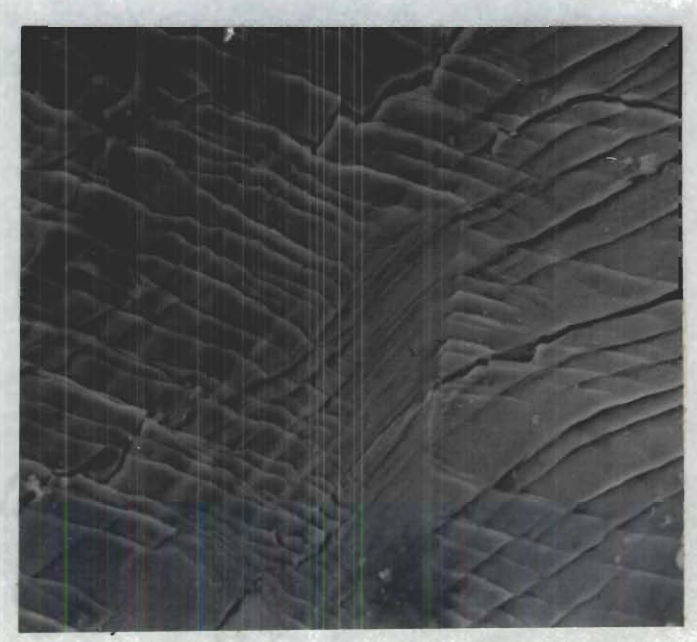

Figure 16. Cracking Associated with Slip Markings on the Surface of an Al-Zn-Mg-Zr 4@120 Fatigue Specimen, $\Delta\varepsilon_p/2 = 4.27\%$. Scanning Electron Micrograph, 570X.

cracks were observed in association with these intense slip markings in the 40120 fatigue specimens, Figure 16. No such cracking was noted in the double-aged specimens in connection with the rather limited surface deformation. Additional cracks at Al-Fe-Si particles and small pits resulting from electropolishing were observed in all specimens. The severity and length of these cracks increased for samples cycled at higher strain amplitudes.

Figure 17 shows typical transmission micrographs of fractured tensile and LCF specimens. Deformation in tensile specimens and LCF specimens cycled at high strain amplitudes resulted in a homogeneous distribution of dislocations, with no evidence of banding. Deformation in LCF specimens cycled at low strain amplitudes also appeared to be homogeneous on a microscopic scale. No specimens exhibited evidence of preferential deformation in precipitate-free zones(PFZ's) adjacent to subgrain boundaries.

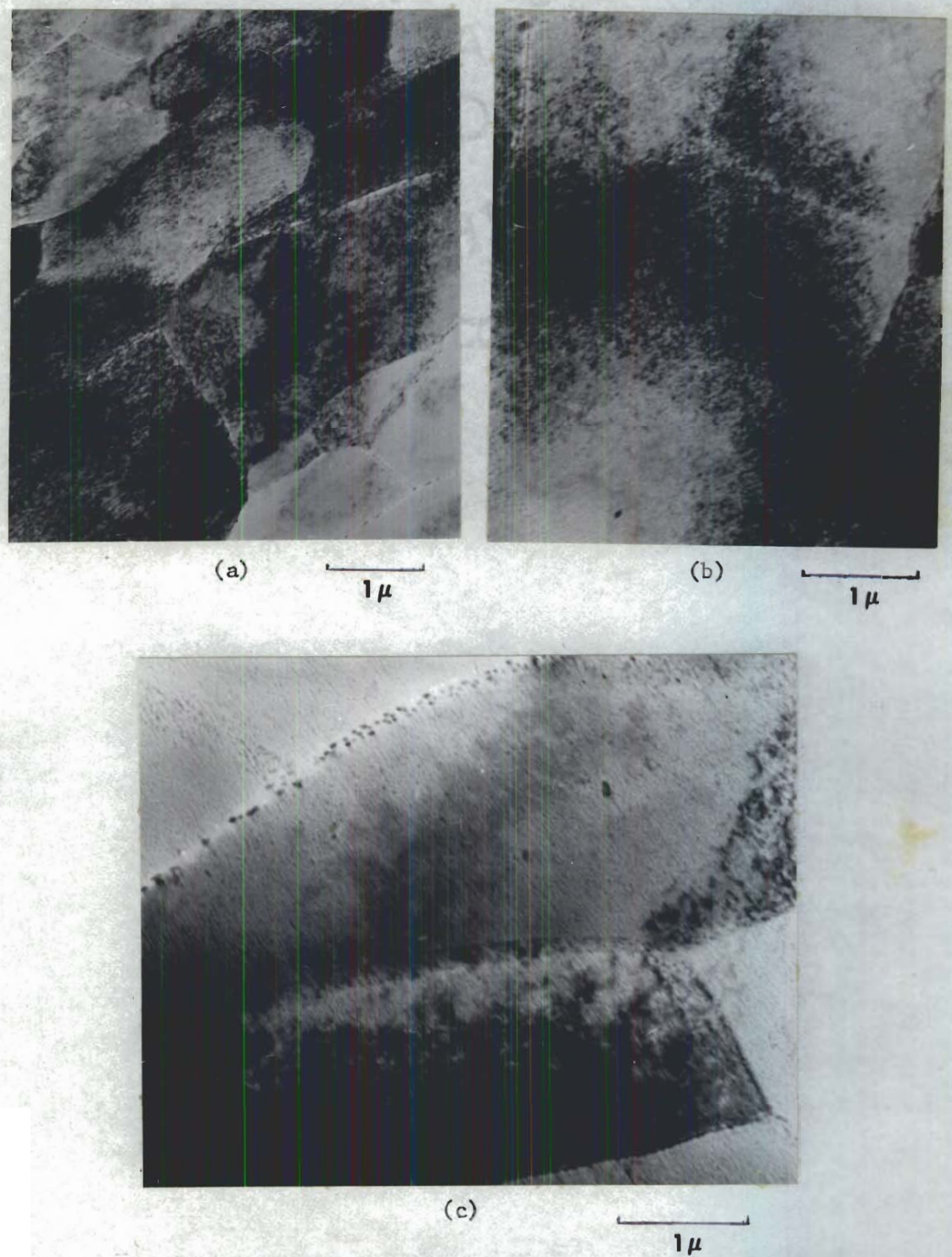

Figure 17. Typical Transmission Electron Micrographs of Al-Zn-Mg-Zr 240 150 Deformed Samples: (a) tensile, (b) fatigue, $\Delta\varepsilon_p/2 = 6.38\%$, and (c) fatigue, $\Delta\varepsilon_p/2 = 0.56\%$.

CHAPTER V

DISCUSSION OF RESULTS

The microstructure of the Al-Zn-Mg-Zr alloy, Figures 1 and 2, shows that the addition of 0.1% zirconium to the Al-Zn-Mg alloy inhibited but did not completely prevent recrystallization and subgrain coalescence for the solution treatment used (1 1/2 hours at 480°C). The zirconium addition did, however, produce a much finer grain structure than that of the Al-Zn-Mg alloy, Figures 9 and 10. Thompson and co-workers[1] extensively studied the use of zirconium as a grain refiner in Al-Zn-Mg-Cu alloys and noted that a large difference in grain sizes could be obtained through a change in homogenization practice. It is evident that the use of zirconium must be accompanied be proper thermal and mechanical treatments to achieve the finest possible grain structure.

The small increases in the yield and ultimate tensile strengths of Al-Zn-Mg-Zr are due simply to a Hall-Petch type relationship analogous to the improvements in fracture toughness observed by the other workers[1]. The refined grain structure of Al-Zn-Mg-Zr reduces dislocation pile-ups and resultant stress concentrations at grain boundaries. This leads to increased ductility and an overall homogenization of deformation, Figures 9 and 10. Microscopically, the brittle intergranular fracture observed in aged large-grained Al-Zn-Mg alloys has been attributed to dislocation bands which produced large stresses across grain boundaries[43]. Such localized deformation bands were observed only in the Al-Zn-Mg alloy in

this study, Figure 12. Homogeneous deformation within grains of the Al-Zn-Mg-Zr alloy led to predominantly transgranular tensile fracture as shown in Figure 11. Bands may have been present in the Al-Zn-Mg-Zr alloy at low strains, but were not observed in TEM foils of fractured (ε_f = 12.8%) tensile specimens, Figure 12, and did not lead to any significant degree of intergranular fracture. In summary, the notable improvements in tensile properties obtained by the addition of zirconium to Al-Zn-Mg may be attributed to the almost complete elimination of grain boundary fracture.

The effect of zirconium on LCF behavior in the Al-Zn-Mg-(Zr) alloys may be analyzed in terms of the difference in grain size. Examination of the cyclic strain hardening exponents, n', Table 4, show that values for Al-Zn-Mg-Zr are approximately twice those observed for Al-Zn-Mg. This correlation between increased n' and increased low cycle fatigue life is in agreement with the analysis by Feltner and Beardmore[33] who suggest that an increase in n' will lead to an increased resistance to cyclic plastic strains and increased low cycle fatigue life. The LCF results for Al-Zn-Mg-(Zr) are also in agreement with the work of Feltner and Laird[19], who showed that n' decreased with decreasing grain size for planar slip materials. The high SFE of Al-Zn-Mg-(Zr) would logically lead to a prediction of a wavy slip mode[23], for which n' is independent of grain size[19]. However, precipitate structures in these alloys limit the occurrence of cross slip, resulting in a planar slip mode for which n' is dependent on the grain size.

Optical and metallographic examination of fatigued specimens revealed that the increase in LCF life for Al-Zn-Mg-Zr, Figure 18, is

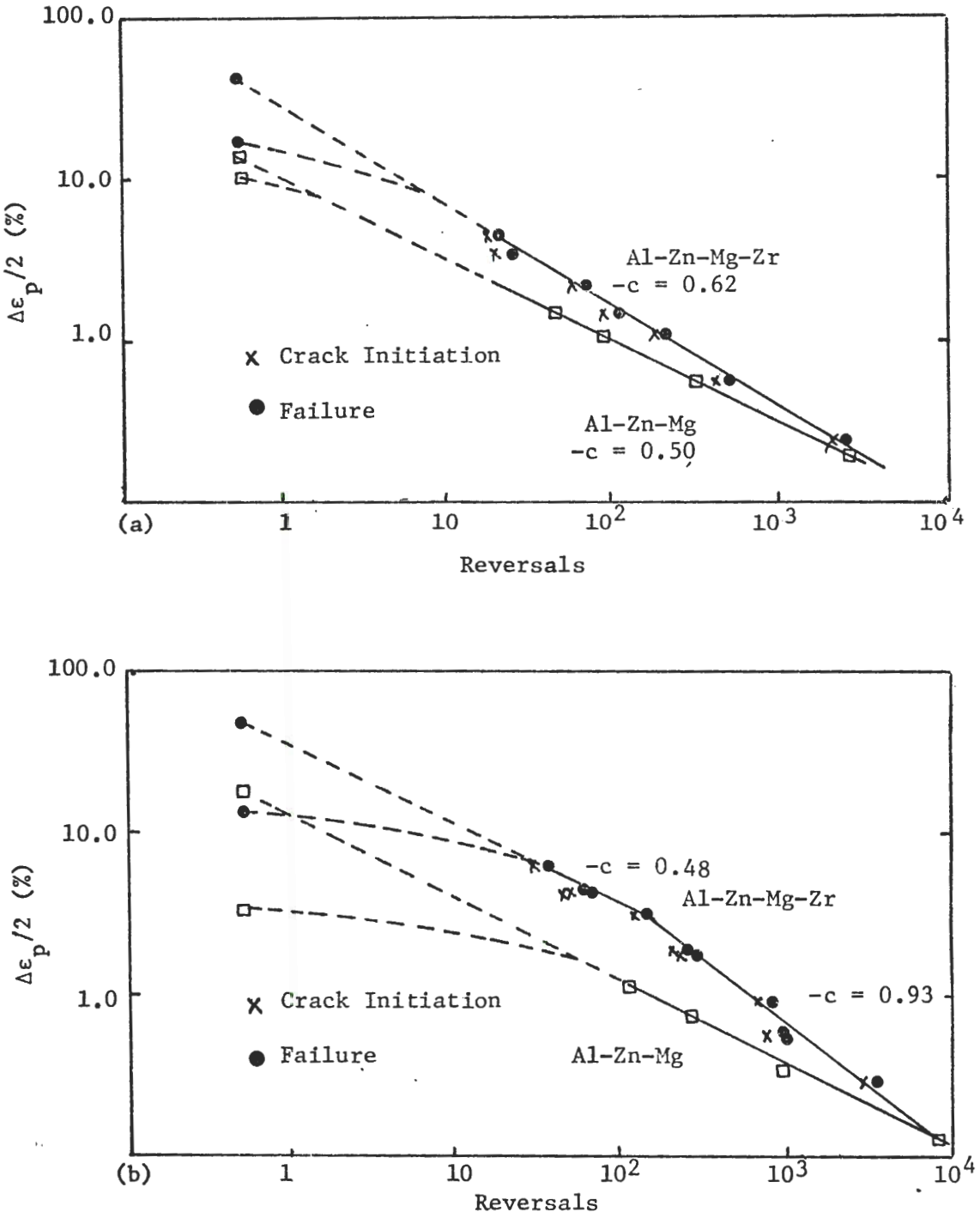

Figure 18. Effect of Grain Size Reduction by Zirconium Addition on LCF of Al-Zn-Mg-(Zr) for Two Aging Conditions: (a) 4@120, and (b) 24@150.

associated with the increased homogeneity of deformation within the grains and the elimination of intergranular fracture, Figures 10c and 13. Microstructurally, the increase in LCF life may be explained in terms of reduced grain boundary offsets developed in the refined Al-Zn-Mg-Zr grain structure at the same levels of plastic strain.[33] For a given grain size, proportional to 1, the plastic strain range can be given by $\Delta\varepsilon_p = \Delta 1/1$. Large-grained materials develop larger offsets, $\Delta 1$, at the grain boundaries than small-grained material, resulting in higher stresses and premature crack initiation. Even though crack initiation data for the Al-Zn-Mg alloy was not available, Figure 18 shows that crack initiation for Al-Zn-Mg-Zr must have occurred much later than for Al-Zn-Mg.

An interesting feature of the comparison of this LCF data is that, by extrapolation of the Coffin-Manson curves (assuming no breaks), a better fatigue resistance is predicted for Al-Zn-Mg at long lives. The lack of ductility in Al-Zn-Mg would not be as detrimental to fatigue life in the high cycle region. The purity of the Al-Zn-Mg alloy is probably beneficial to its high cycle fatigue resistance when compared to Al-Zn-Mg-Zr. The presence of Al-Fe-Si intermetallics in Al-Zn-Mg-Zr may contribute to earlier crack initiation[44] and failure than observed in "cleaner" alloys. Though the Al-Zn-Mg-Zr alloy is undoubtably superior to Al-Zn-Mg in the high-strain LCF range, its capacities to resist fatigue would certainly be improved by achievement of a more homogeneous fine-grained microstructure. Inhomogeneous microstructures such as that observed for Al-Zn-Mg-Zr lead to an inhomogeneous distribution of strain. Deformation tends to occur preferentially in larger recrystallized grains, where strengthening

effects due to grain boundaries are not present. Depending upon slip mode, deformation may become concentrated in planar dislocation bands, a condition known to be conducive to intergranular fracture and detrimental to fatigue crack initiation resistance. Recent research at Alcoa[45] indicates that partially recrystallized microstructures similar to that of Al-Zn-Mg-Zr show fatigue properties inferior to similar fully recrystallized or fully unrecrystallized commercial alloys. Thermomechanical processing[46,47] has been used successfully to produce very homogeneous, fine recrystallized grain structures, which may be beneficial in improving fatigue resistance[1].

Figure 19 gives a comparison of the effect of aging treatment on LCF life of Al-Zn-Mg-Zr as expressed by the Coffin-Manson relation. The poorest LCF life for the range of plastic strain amplitudes studied was shown by samples aged 4 hours at 120°C, an underaged condition. For this aging treatment, small coherent GP zones (R_G = 23A) are sheared by dislocations, resulting in a planar slip mode. Cross slip is difficult and dislocations tend to remain confined to a single glide plane. Cyclic hardening, Figure 4a, occurs by the multiplication and entanglement of dislocations on these glide planes. Slip reversibility becomes more limited as hardening continues, and crack initiation occurs due to the development of a notch-peak topography on the specimen surface. Such cracks initiated on the surface of 4@120 fatigue specimens are shown in Figure 16. LCF results for the double-aging treatments, which produce high densities of η' and η precipitates[4], show increased life compared to 4@120 samples. These increases in LCF resistance are due to the

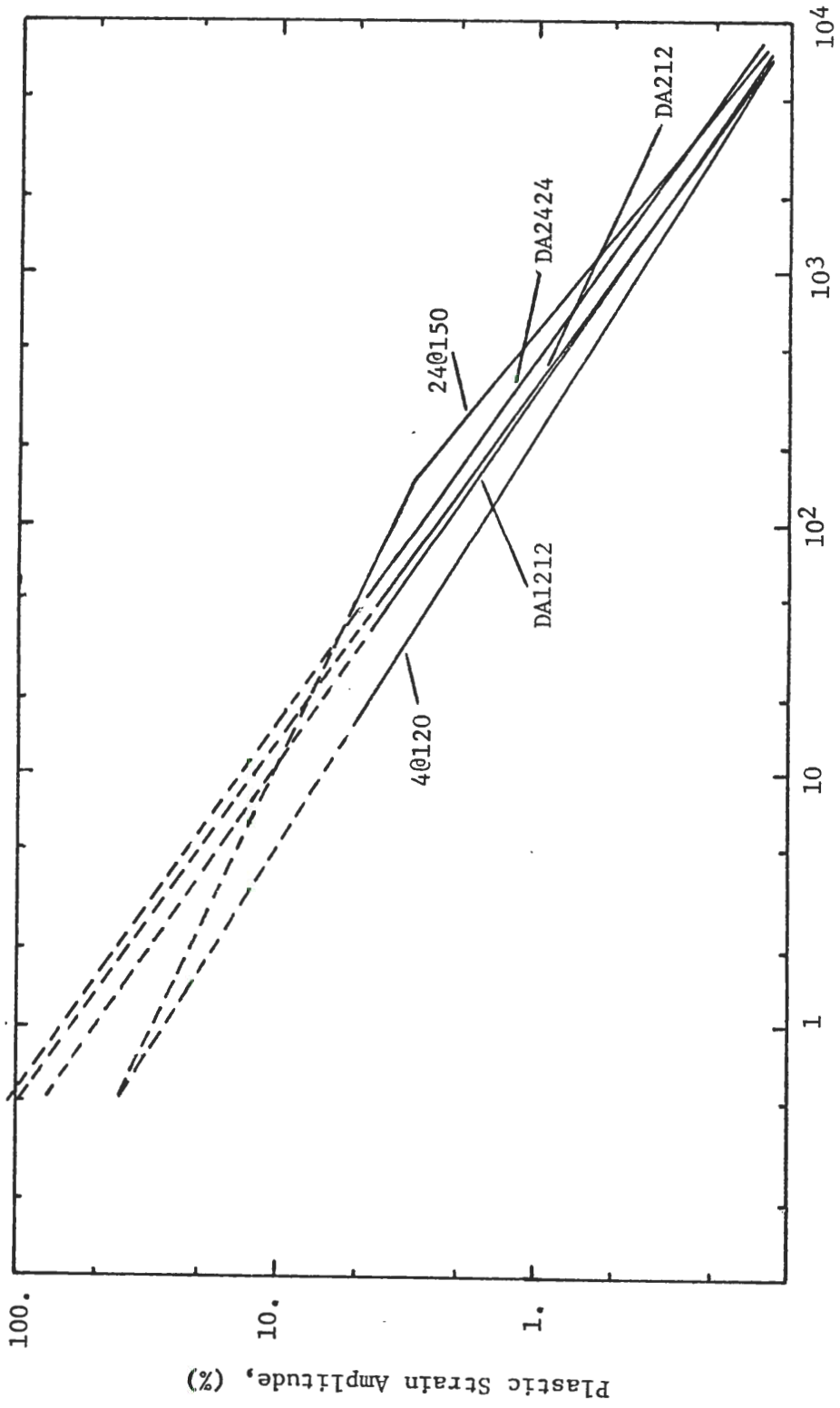

Figure 19. Effect of Aging Treatment on LCF Life of Al-Zn-Mg-Zr.

increased occurrence of dislocation looping at incoherent η particles. Shearing of semicoherent η' may still occur to some degree because of the high particle density. However, the slip mode is less planar than the underaged treatment, 4@120, and cyclic hardening due to dislocation tangles on individual glide planes is not as pronounced. Overall deformation within grains is more homogeneous and the development of a notch-peak topography preceding crack initiation is difficult. Samples aged 24 hours at 150°C, an overaged condition, exhibited the best LCF life observed for the range of plastic strain amplitudes studied. A similar improvement in LCF life noted by Selines[3] for 7075 was attributed to the increase in fracture toughness of the overaged condition. However, fracture toughness is related to critical crack growth resistance, and has been shown to be inadequate for predicting fatigue resistance[1,48]. For the present investigation, the improved LCF life for the 24@150 aging treatment is more probably related to an improved homogeneity of deformation resulting from dislocation looping of incoherent η particles.

Extrapolation of the Al-Zn-Mg-Zr LCF results to long lives (>10^5 cycles) would indicate that the underaged 4@120 treatment would have superior fatigue life in the high cycle fatigue region. S-N curves would be necessary to determine this effect unambiguously. However, results for Al-Cu-Mg alloys[49] show that fatigue strength is increased in underaged structures exhibiting a shear-type deformation mode, an effect possibly associated with improved reversibility of slip. Actually, a combination of deformation mechanisms may be necessary for resistance to both high and low cycle fatigue. Fine[2] has proposed that a duplex structure,

containing shearable particles for high strength and nondeformable particles to homogenize deformation, may lead to improved fatigue-resistant alloys.

A comparison was made of the experimental LCF parameters, c and ε'_f, obtained for Al-Zn-Mg-Zr and various theoretical predictions found in the literature. Table 5 shows that only the Morrow[50] correlation between n', the cyclic strain hardening exponent, and c for the double-aged treatments is adequate. None of the proposed correlations for predictions of ε'_f appear to be reasonable. The failure of these and other such theoretical predictions has been noted previously[3] and has led to the generalization that aluminum alloys show marked deviations from the Coffin-Manson relationship.[10,35]

The Coffin-Manson plots of similarly aged Al-Zn-Mg-Zr and 7050, Figure 20, show that Al-Zn-Mg-Zr exhibited better fatigue life than 7050 for the range of plastic strain amplitudes studied. The higher strength levels and slightly reduced ductility of 7050 may be partially responsible for this effect since ductility has been shown to be an important factor in determining LCF resistance. However, some significant differences in microstructure may contribute significantly to these results:

1. Grain Structure - The processing and resultant microstructures of Al-Zn-Mg-Zr and 7050 are different. The 7050 structure appears to be more completely recrystallized. The exact effect of this difference is unknown.

2. Precipitate Structure - Copper present in 7050 has been shown to enter directly into GP zone formation and promote η' nucleation from GP zones at earlier aging times[4] producing a higher volume fraction of η' in 7050 than in Al-Zn-Mg-Zr for a given aging treatment. This larger particle

Table 5. Comparison of Experimentally Obtained LCF Parameters with Various Theoretical Predictions

Low Cycle Fatigue Parameter	4@120	24@150	DA212	DA1212	DA2424
n'	.086	.102	.092	.091	.094
c (experimental)	-.62	-.48 -.92	-.71	-.69	-.70
$c = -1/(1+5n')$ Morrow[50]	-.70	-.66	-.68	-.69	-.68
$c = -1/(1+2n')$ Tomkins[8]	-.85	-.83	-.84	-.86	-.84
ε'_f (experimental)	.43	.48 6.32	.98	.69	1.16
ε_f (from tensile test)*	.172	.143	.129	.128	.141
$\varepsilon_f = \ln(A_o/A_f)$ Morrow[51]	.38	.61	.51	.48	.56
$\varepsilon_f = .51\ln(A_o/A_f)$ Manson[52]	.19	.31	.26	.24	.28

*calculated from $\varepsilon_f = \ln(1+e_f)$, where e_f = elongation to fracture

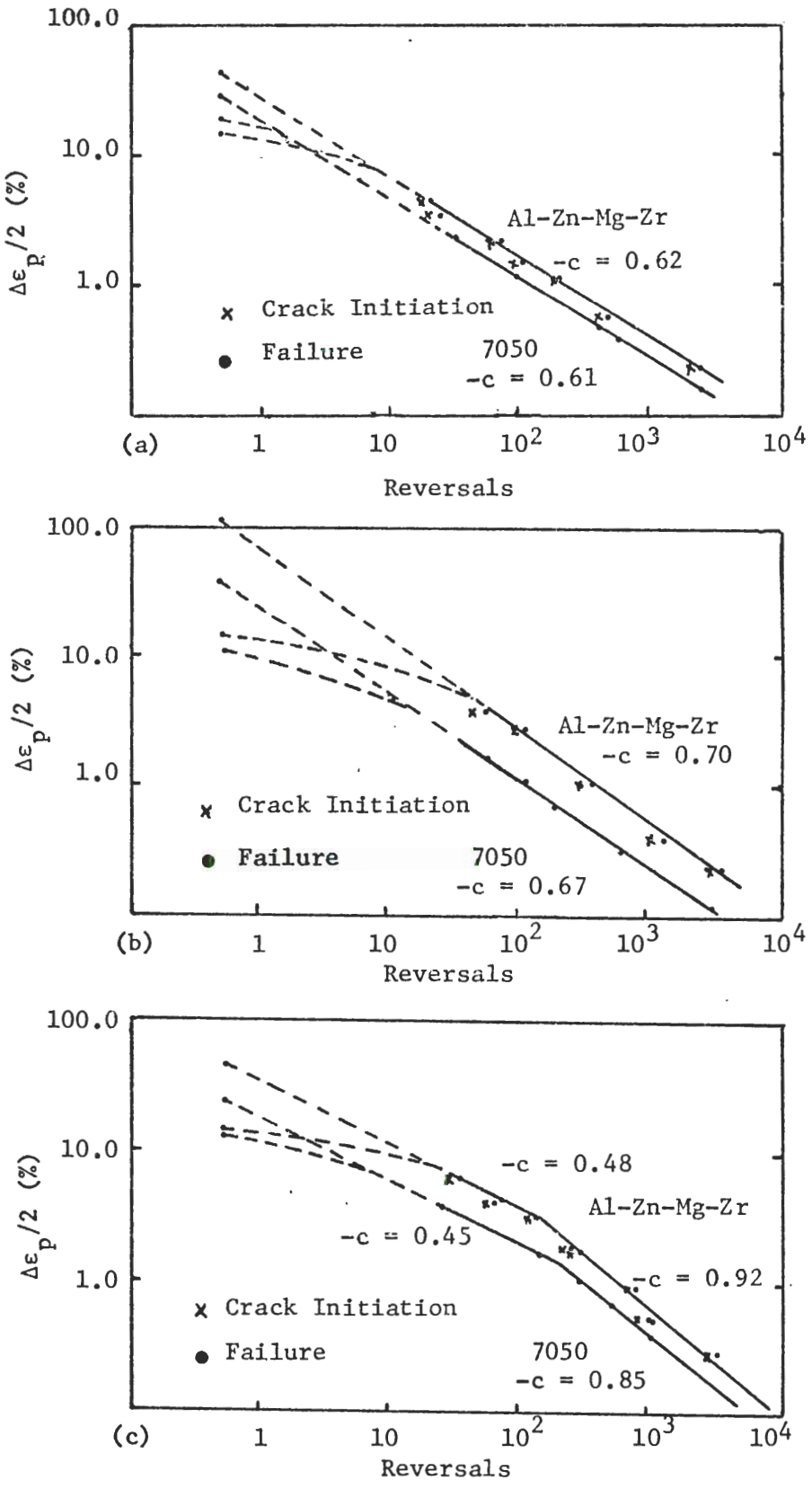

Figure 20. Comparison of LCF Data of Al-Zn-Mg-Zr and 7050 for Three Aging Conditions: (a) 4@120, (b) DA 2424, and (c) 24@150.

density in 7050 may result in earlier crack initiation according to the model of Duquette and Swann[53]. They proposed that portions of dislocations, forced to cross slip out of the primary slip plane by interactions with precipitates, combined with point defects generated during fatigue to form dipolar dislocation loops across the primary slip plane. The higher particle density in the 7050 alloy would generate larger numbers of dislocation loops and result in earlier initiation of fracture than in the lower particle density Al-Zn-Mg-Zr alloy for the aging treatments where dislocation looping is observed.

3. Cu - rich Intermetallics - The presence of insoluble copper-rich intermetallic particles has been identified in 7050[1,4] and may act as sites for crack initiation. Their possible detrimental effect on crack propagation has also been noted[3,4] and Alcoa's newer 7050 alloys have reduced copper content to eliminate these insoluble particles.

4. Al-Fe - Si Inclusions - The 7050 alloy had slightly higher contents of Fe and Si. As mentioned previously, Al-Fe-Si particles have been observed as sites for crack initiation in Al alloys[44].

The complexities of the microstructural differences and the lack of comparable crack initiation data makes an unambiguous comparison of the 7050 and Al-Zn-Mg-Zr data impossible. Studies of the effect of copper on the LCF behavior of these alloys have been undertaken on alloys of similar grain structure, aged to comparable strength levels, and should provide more conclusive answers to these questions.

The failure of the Coffin-Manson relation to predict the LCF life of Al-Zn-Mg-Zr aged 24 hours at 150°C, Figure 5b, appears to be related to fatigue deformation processes prior to crack initiation. The 24@150 LCF data, plotted as plastic strain amplitude versus number of reversals to crack initiation ($2N_i$) in Figure 20 shows a discontinuity in slope analogous to that of the $\Delta\varepsilon_p/2$ -$2N_f$ relationship. Santner and Fine[54] reported similar results for Al-3.6 Cu and 2024 when plots of $\Delta\varepsilon_p/2$ vs.

$2N_f$ and $\Delta\varepsilon_p/2$ vs. $2N_i$ were compared. An SEM examination of Al-Zn-Mg-Zr 24@150 fatigue specimen fracture surfaces, Figure 14, showed that the crack propagation process was essentially the same, regardless of plastic strain amplitude. This observation does not support the work of other investigators, who have cited changes in crack propagation mode[9] or increased secondary cracking[36] at low plastic strain amplitudes to explain the change in fatigue ductility exponent. The SEM results of the present investigation indicate that the change in slope of the Coffin-Manson plot of the Al-Zn-Mg-Zr 24@150 data is related to the crack initiation, rather than the crack propagation, process.

The plastic work per unit volume, W_p, is a measure of the energy absorbed by a sample prior to crack initiation in a LCF test. The value of W_p, as calculated from Equation 4, may be related to the capacity of a microstructure to resist cyclic deformation before a fatal crack is initiated.

$$W_p = \sum_{i=1}^{N_i} \Delta\sigma\Delta\varepsilon_p \qquad (4.)$$

where

$\Delta\sigma$ - is the applied stress range,

$\Delta\varepsilon_p$ - is the plastic strain range,

and

N_i - is the number of cycles for crack initiation.

Plots of W_p vs. N_i for three aging treatments are shown in Figure 21. The data appears to fit an essentially linear plot for samples of the 4@120 aging treatment, while the 24@150 and DA2424 data have distinct breaks

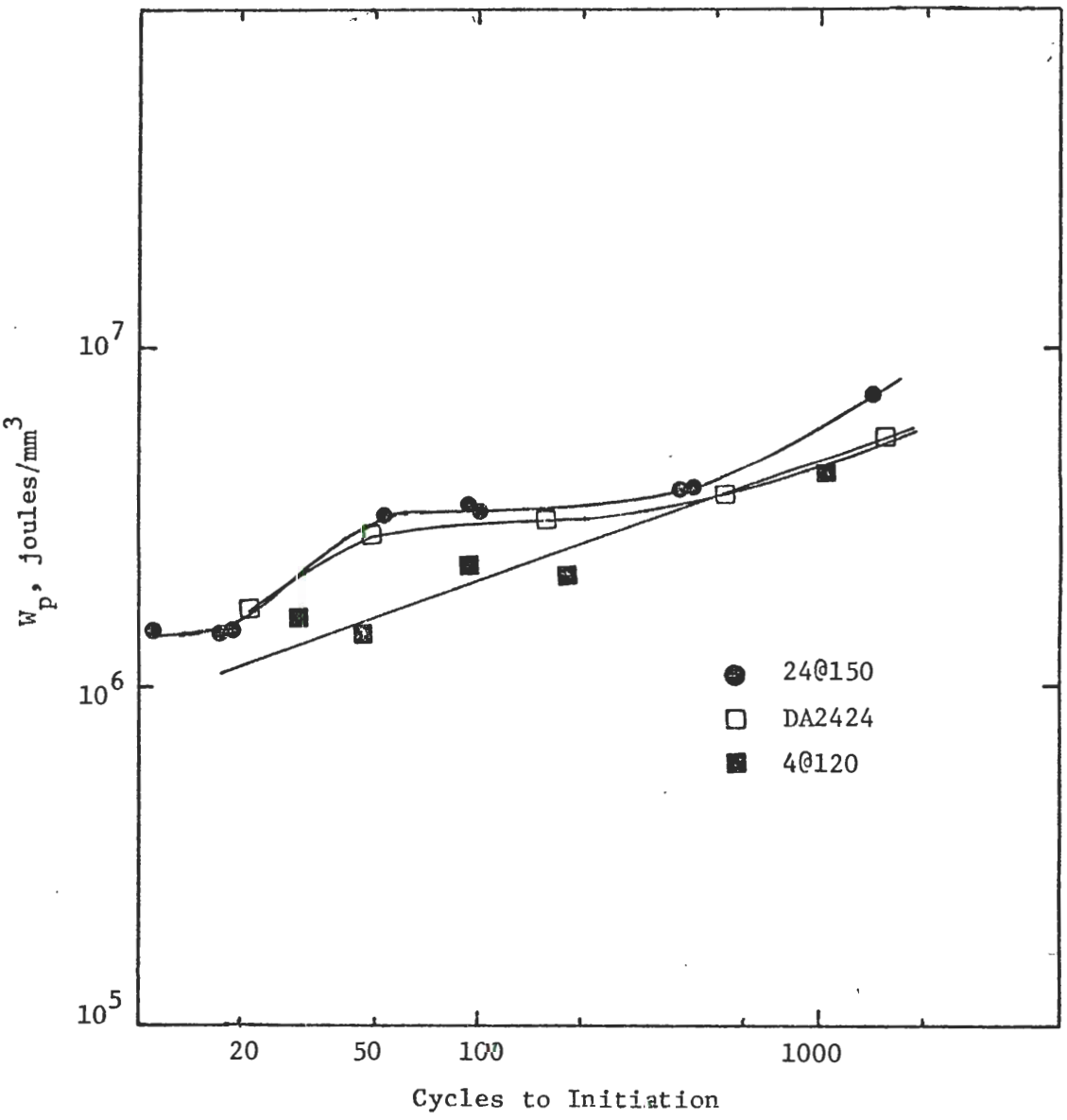

Figure 21. Plot of Plastic Work versus Number of Cycles to Crack Initiation for: (a) 24@150, (b) 4@120 and (c) DA2424.

in slope at approximately N_i = 50 cycles. The amount of energy absorbed by samples prior to crack initiation at high strain amplitudes (low N_i) is considerably smaller than predicted by extrapolation from W_p at lower strain amplitudes for these two aging treatments. (Had data for DA2424 samples been taken at lower values of N_i, more distinct breaks may have been noted in plots of both W_p vs. N_i and $\Delta\varepsilon_p/2$ vs. $2N_f$.) Interpreted as a change in fatigue resistance with strain amplitude, this distinct break in the W_p vs. N_i curve correlates well with the change in slope of the Coffin-Manson plot for samples of the 24@150 aging treatment.

Samples of the other aging treatments studied were probably not fatigued at strain amplitudes large enough to note such deviations in their Coffin-Manson plots, as shown in Figures 18-20. By cyclically straining at sufficiently large $\Delta\varepsilon_p/2$, breaks in the Coffin-Manson plots of all LCF data where $\varepsilon_f' > \varepsilon_f$ must necessarily be observed since the value of ε_f sets an absolute upper limit for $\Delta\varepsilon_p/2$. This analysis is supported by the observations of many workers who studied LCF properties of aluminum alloys[4,6,10,35].

A TEM examination of foils taken from Al-Zn-Mg-Zr 24@150 fatigue specimens, Figure 17, was made in an attempt to relate the change in slope of the Coffin-Manson plot to possible microstructual effects on deformation. No evidence of inhomogeneous deformation at low plastic strain amplitudes (cited by other workers[4,39] as the probable cause of premature crack initiation and the break in the Coffin-Manson plot) was noted in this study. The TEM evidence in a previous investigation[4] was obtained from foils taken within 0.5mm of the fracture surface. Dislocation structures in this region may have been more indicative of the fatigue

microstructures responsible for crack initiation, and ultimately, for the deviation in the Coffin-Manson plot. However, the proximity of the foils to the fracture surface may have placed them inside the region influenced by the plastic zone of the growing fatigue crack, and led to observations of dislocation structures typical of fatigue crack growth. A subsequent investigation[39], in which foils were taken well away from the fracture surface, reported dislocation banding at low plastic strain amplitudes as the cause of premature crack initiation in aluminum alloys. More extensive studies of the influence of microstructure on the non-linearity of the Coffin-Manson plot are anticipated, with the final goal of isolating the particular feature(s) responsible for this effect.

CHAPTER VI

CONCLUSIONS

1. Solution heat treatment of the Al-Zn-Mg-Zr alloy at 480°C for 1 1/2 hours results in a partially recrystallized microstructure due to the presence of zirconium as a grain refiner.
2. The presence of 0.1% zirconium does not affect the aging kinetics of the Al-Zn-Mg-Zr alloy composition studied.
3. The greatly increased ductility and virtual elimination of brittle fracture observed in Al-Zn-Mg-Zr is due to the increased homogeneity of deformation resulting from the grain size refinement. Brittle intergranular fracture in Al-Zn-Mg is due to the presence of inhomogeneous deformation bands.
4. The refined grain structure of Al-Zn-Mg-Zr produces more homogeneous deformation, leading to smaller stress concentrations at grain boundaries, and resulting in improved resistance to crack initiation and failure in the LCF region.
5. A microstructure consisting of large η particles produced by aging for 24 hours at 150°C, exhibits the best LCF resistance of the aging treatments studied due to the increased incidence of dislocation looping which results in more homogeneous deformation.
6. Several theoretical relationships did not adequately predict the LCF parameters, c and ε'_f, for Al-Zn-Mg-Zr due to the characteristic failure of the Coffin-Manson relation to predict LCF behavior of

aluminum alloys at high plastic strain amplitudes.

7. The failure of the Coffin-Manson relation to predict the LCF behavior of Al-Zn-Mg-Zr aged 24 hours at 150°C over the fatigue life range studied is related to a change in fatigue deformation with plastic strain amplitude prior to crack initiation.

APPENDIX A

Low Cycle Fatigue Data of Al-Zn-Mg-Zr Alloy

Aging Treatment	$\Delta\varepsilon_p/2$	Cycles for Saturation	Cycles for Crack Initiation	Cycles for Failure
4@120	0.23	900	1060	1225
	0.56	170	210	250
	1.14	78	95	109
	2.22	26	30	39
	3142	6	10	13
DA212	0.12	1200	2350	2740
	0.44	190	285	360
	0.78	70	170	209
	1.22	15	95	131
	2.78	7	22	36
	4.57	5	14	21
DA1212	0.20	700	1300	1749
	0.31	290	525	640
	0.87	60	145	181
	1.32	20	105	133
	2.81	9	34	43
	3.74	3	13	19
DA2424	0.24	800	1510	1903
	0.40	156	520	692
	1.07	65	153	207
	2.80	8	50	63
	3.79	5	23	30
24@150	0.30	1	1400	1705
	0.58	1	370	498
	0.91	12	345	416
	1.89	10	108	129
	3.14	10	61	74
	4.11	4	23	34
	4.19	3	25	30
	6.38	3	15	18

BIBLIOGRAPHY

1. D. S. Thompson and R. E. Zinkham: "Research on Synthesis of High-Strength Aluminum Alloys," Technical Report AFML-TR-74-129, Part I.

2. M. E. Fine: Met. Trans., 1975, Vol. 6A, p. 625

3. R. J. Selines: Ph. D. Thesis, 1974, Massachusetts Institute of Technology, Cambridge, Mass.

4. T. H. B. Sanders, Jr., and E. A. Starke, Jr.: Met. Trans. (in press).

5. J. F. Tavernelli and L. F. Coffin, Jr.: Trans. ASM, 1959, Vol. 51, pp. 438-50.

6. S. S. Manson and M. H. Hirschberg: "Fatigue Behavior in Strain Cycling in the Low- and intermediate-Cycle Range," Fatigue: An Interdisciplinary Approach, p. 133, Syracuse University Press, Syracuse, N. Y., 1964.

7. A. Saxena and S. D. Antolovich, to be published.

8. B. Tomkins: Phil. Mag., 1968, Vol. 18, p. 1041.

9. L. F. Coffin, Jr.: J. of Materials, JMLSA, 1971, Vol. 6, pp. 388-402.

10. L. F. Coffin, Jr.: Proc. of Symposium on Internal Stresses and Fatigue in Metals, Elsevier Publishing Co., New York, N. Y., 1959, pp. 363-381.

11. R. W. Armstrong: Adv. in Mat. Research, IV, Wiley-Intenscience, N. Y., 1969, p. 101.

12 G. M. Sinclair and W. J. Craig: Trans. ASM, 1952, Vol. 44, p. 929.

13. R. P. Carreker: Trans. ASM, 1952 Vol. 44, p. 946.

14. E. O. Hall: Proceedings Physical Society, 1951, Vol. B64, p. 742.

15. H. Okubo, S. Murakami, and K. Hosono: J. Inst. Metals, 1962-63, Vol. 91, p. 95.

16. M. Klesnil, M. Holtzmann, P. Lukas, and P. Rys: J. Iron Steel Inst., 1965, Vol. 203, p. 47.

17. P. G. Forrest and A. E. L. Tate: J. Inst. Metals, 1964-65, Vol. 93, p. 438.

18. C. E. Feltner and C. Laird: Trans. TMS - AIME, 1969, Vol. 245, p. 1372.

19. C. E. Feltner and C. Laird: Acta. Met., 1967, Vol. 15, p. 1621.

20. C. E. Feltner and C. Laird: Acta. Met., 1967, Vol. 15, p. 1633.

21. J. C. Grosskreutz: Phys. Stat. Sol. (b), 1971, Vol. 47, p. 359.

22. D. H. Avery, G. A. Miller, and W. A. Backofen: Acta. Met., 1961, Vol. 9, p. 892.

23. R. M. Pelloux: "Influence of Grain Size on Fatigue," Ultrafine Grain Metals, p. 231, Syracuse University Press, Syracuse, N. Y., 1970.

24. A. W. Thompson and W. A. Backofen: Acta. Met., 1971, Vol. 19, p. 597.

25. R. C. Boettner, C. Laird, and A. J. McEvily: Trans. TMS-AIME, 1965, Vol. 233, p. 374.

26. G. A. Miller, D. H. Avery, and W. A. Backofen: Trans. TMS-AIME, 1966, Vol. 236, p. 1667.

27. B. Z. Weiss, S. Niedzwiedz, and M. Breur: J. Iron Inst., 1966, Vol. 204, p. 152.

28. C. Laird and G. C. Smith: Phil. Mag., 1963, Vol. 8, p. 1945.

29. C. Laird and C. E. Feltner: Trans. TMS-AIME, 1967, Vol. 239, p. 1074.

30. R. P. Carreker and W. B. Hibbard: Acta. Met., 1953, Vol. 1, p. 654.

31. T. L. Johnston and C. E. Feltner: Met. Trans., 1970, Vol. 1, p. 1161.

32. C. Laird and C. E. Feltner: Trans. TMS-AIME, 1967, Vol. 239, p. 1074-1083.

33. C. E. Feltner and P. E. Beardmore: "Strengthening Mechanisms in Fatigue," Achievement of High Fatigue Resistance in Metals and Alloys, ASTM STP 467,American Society for Testing and Materials, 1970, pp. 77-112.

34. A. C. Low: International Conference on Fatigue of Metals, London, Session 2, 1956, Paper 15.

35. T. Endo and J. Morrow: J. of Materials, JMLSA, 1969, Vol. 4, pp. 159-175.

36. B. Tomkins: Phil. Mag., 1971, Vol. 23, P. 687.

37. C. Calabrese and C. Laird: Met. Trans., 1974, Vol. 5, p. 1785.

38. D. E. Martin: J. of Basic Eng. (Trans. ASME), 1965, Vol. 87, series D, p. 850.

39. T. H. B. Sanders, Jr., D. A. Mauney, and J. T. Staley: 10th Annual Symposium on Materials Science, ed. R. I. Jaffee, 1975, (in press).

40. V. Gerold: "Applications of Small-Angle X-ray Scattering to Problems In Physical Metallurgy and Metal Physics," X-Ray Small Angle Scattering, ed. H. Brumberger, Gordon and Breuch, New York, 1967, pp. 277-317.

41. American Society for Testing and Materials: "Tension Testing of Metallic Materials," 1974 Book of ASTM Standards, Designation E 8-69, 1974, p. 90.

42. Sandor, B. I.: Fundamentals of Cyclic Stress and Strain, Univ. of Wisconsin Press, Madison, 1972.

43. N. Ryum, B. Haegland, and T. Lindtveit: Z. Metallkde, 1967, Vol. 58, p. 28.

44. S. Pearson: Eng. Fract. Mech., 1975, Vol. 7, p. 235.

45. T. H. Sanders, Jr., Alcoa Technical Center, 1976, private communication.

46. J. Waldman, H. Sulinski, and H. Markus: Met. Trans., 1974, Vol. 5, p. 573.

47. Di Russo, M. Conserva, F. Gatto, and H. Markus: Met. Trans., 1973, Vol. 4, p. 1133.

48. C. F. Babilon, R. H. Wygonik, G. E. Nordmark, and B. W. Lifka: "Mechanical Properties, Fracture Toughness, Fatigue, Environmental Fatigue Crack Growth Rates and Corrosion Resistance of High-Toughness Aluminum Alloy Forgings, Sheet, and Plate," Technical Report AFML-TR-73-83, April, 1973.

49. J. M. Finney: Mater. Sci. Eng., 1970, Vol. 6, p. 55.

50. J. Morrow: Internal Friction, Damping, and Cyclic Plasticity, ASTM 378, 1965, p. 45.

51. J. Morrow: Fatigue Design Handbook, SAE, New York, 1968, Chapt. 3.2.

52. S. S. Manson: Machine Design, MADEA, 1961, p. 165.

53. D. J. Duquette and P. R. Swann: "An Electron Microscopic Examination of Pre-Crack Fatigue Damage in Age-Hardened Al-5Zn-2.5Mg", ONR Tec. Rept. 3, Feb., 1974.

54. J. Santner and M. E. Fine: Met. Trans. (in press).